# THE DEVELOPMENT OF FORMING SIMULATION METHODOLOGY OF A PLATE TYPE HEAT EXCHANGER

**A Thesis Submitted to**
**the Graduate School of**
**İzmir Institute of Technology**
**in Partial Fulfillment of the Requirements for the Degree of**

**MASTER OF SCIENCE**

**in Mechanical Engineering**

**by**
**İbrahim ŞİMŞEK**

**July 2023**
**İZMİR**

We approve the thesis of **İbrahim ŞİMŞEK**

**Examining Committee Members:**

**Prof. Dr. Alper TAŞDEMİRCİ**
Department of Mechanical Engineering, İzmir Institute of Technology

**Prof. Dr. Hatice Seçil ARTEM**
Department of Mechanical Engineering, İzmir Institute of Technology

**Prof. Dr. Evren Meltem TOYGAR**
Department of Mechanical Engineering, Dokuz Eylül University

**5 July 2023**

**Prof. Dr. Alper TAŞDEMİRCİ**
Supervisor, Department of
Mechanical Engineering,
İzmir Institute of Technology

**Prof. Dr. M. İ. Can DEDE**
Head of the Department of
Mechanical Engineering

**Prof. Dr. Mehtap EANES**
Dean of the Graduate School

# ACKNOWLEDGMENTS

I would like to express my gratitude to Prof. Dr. Alper TAŞDEMİRCİ for his patience and guidance. This study would have never been accomplished without his inspiration and encouragement.

I would like to thank Bosch Termoteknik Manisa Plant R&D department for providing resources and support for this study.

I wish to thank to IZTECH Dynamic Testing and Modelling Laboratory, Atılım University, fka GmbH and Simultra Material Technologies for the test results they provided.

I owe gratefulness to my colleagues at Bosch Termoteknik Manisa Plant R&D Department; Yiğit GÜRLER, Berkay Türkcan İMRAĞ, and Çağatay KÖK for their support.

I would like to thank all of my friends at the IZTECH Dynamic Testing and Modelling Laboratory; Mehmet Yalçın SIRMALILAR and Mesut BAYHAN for their valuable support, and association.

I am deeply grateful to my mother Kevser ŞİMŞEK, my father Ramazan ŞİMŞEK, my brother Berkin ŞİMŞEK for their financial and emotional support throughout my education life.

I owe gratefulness to my love Simay SEÇGİN for her emotional support throughout my education life.

# ABSTRACT


## THE DEVELOPMENT OF FORMING SIMULATION METHODOLOGY OF A PLATE TYPE HEAT EXCHANGER

In this study, the production process of plate type heat exchangers was developed as a simulation methodology. Within the scope of the study, first, the parameters in the production process were determined. Then, mechanical characterization studies were planned with the AISI 316L stainless steel material used during production and the alternative AISI 304 stainless steel material, and the tests were completed with the support of the relevant stakeholders. The tests were determined according to the requirements of the simulation methodology. In this context, uniaxial tensile test, biaxial hydraulic bulge test and Split Hopkinson tensile tests were performed to obtain the necessary inputs for the mechanical characterization of the material and creating the material model. The material models established with the information obtained from the tests were validated with the modeling of the test setups in the numerical environment. The simulation methodology was developed in the LS-DYNA environment in the light of the process parameters obtained from the production and the data obtained from the mechanical characterization tests. The simulation model created with the developed methodology was verified because of comparison with the sample produced from AISI 316L stainless steel material taken from production. After the verified model was obtained, a simulation model was created with AISI 304 stainless steel. In addition, for the model formed with AISI 316L stainless steel, process parameters optimization study was carried out, and preliminary work activities related to reducing production times were carried out in numerical environment. After these modeling activities, the knowledge of the license plate was increased. In addition, effective plastic stress during the process, springback effect, residual stress values after springback, effective plastic strain, thickness distribution and thickness reduction values were obtained for the plate. By using the forming limit diagram of AISI 316L stainless steel, information about the final formability behavior was obtained.

# ÖZET

## PLAKA TİPİ ISI EŞANJÖRÜNÜN ŞEKİLLENDİRME SİMÜLASYON METODOLOJİSİNİN GELİŞTİRİLMESİ

Bu çalışmada, plaka tipi ısı eşanjörlerinin üretim prosesi simulasyon metodolojisi olarak geliştirilmiştir. Yapılan çalışma kapsamında öncelikle üretim prosesindeki parametreler tespit edilmiştir. Ardından üretim esnasında kullanılan AISI 316L paslanmaz çelik malzemesi ve alternatif olarak seçilen AISI 304 paslanmaz çelik malzemesi ile mekanik karaekterisazyon çalışmaları planlandı ve testler ilgili paydaşların desteği ile birlikte tamamlandı. Yapılan testler, simulasyon metodolojisinin isterlerine göre belirlendi. Bu bağlamda tek eksenli çekme testi, çift eksenli hidrolik çıkıntı testi ve Split Hopkinson çekme testleri gerçekleştirilerek, malzemenin mekanik karekterizasyonu ve malzeme modelini oluşturmak için gerekli girdiler elde edildi. Testlerden elde edilen bilgiler ile kurulan malzeme modelleri, test setuplarının nümerik ortamda modellenmesi ile birlikte doğrulandı. Üretimden elde edilen proses parametreleri ve mekanik karekterisazyon testlerin elde edilen verilerin ışığında simulasyon metodolojisi LS-DYNA ortamında geliştirildi. Geliştirilen metodoloji ile oluşturulan simulasyon modeli, üretimden alınan AISI 316L paslanmaz çelik malzemesinden üretilen numune ile karşılaştırılması sonucunda doğrulandı. Doğrulanmış model elde edildikten sonra AISI 304 paslanmaz çeliği ile de simulasyon modeli oluşturuldu. Ayrıca, AISI 316L paslanmaaz çeliği ile oluştutrulan model için proses parametreleri optimizasyon çalışması yapılarak, üretim sürelerinin azaltılması ile ilgili ön çalışma faaliyetleri nümerik ortamda gerçekleştirildi. Bu yapılan modelleme faaliyetleri sonrasında, plakalı özelinde bilgi birikimi arttırılmıştır. Buna ilaveten plakalı ile ilgili, proses sırasındaki etkin plastik gerilme, geri esneme etkisi, geri esneme sonrası artık gerilme değerleri, etkili plastik gerinim, kalınlık dağılımı ve kalınlık azaltma değerleri elde edilmiştir. AISI 316L paslanmaz çeliğinin şekillendirme limit diyagramı kullanılarak, nihai şekillendirilebilirlik davranışları hakkında bilgiler elde edilmiştir.

# TABLE OF CONTENTS

LIST OF THE FIGURES ..... viii

LIST OF TABLES ..... xi

CHAPTER 1. INTRODUCTION ..... 1

1.1. Problem Definition and Aim of the Study ..... 6

CHAPTER 2. LITERATURE ..... 8

2.1. Literature Survey ..... 8

CHAPTER 3. THEORY ..... 14

CHAPTER 4. MECHANICAL CHARACTERIZATION ..... 21

4.1. Uniaxial Tensile Test ..... 21

4.2. Hydraulic Bulge Test ..... 25

4.2.1. Nakajima Tests FLD (Forming Limit Diagram) ..... 27

4.3. Dynamic Test ..... 28

4.3.1. Split Hopkinson Pressure Bar Tension Test ..... 28

4.4. Material Model ..... 31

4.4.1. Material Parameters ..... 33

CHAPTER 5. NUMERICAL MODELLING ..... 35

5.1. Finite Element Analysis (FEA) ..... 35

5.1.1. LS-DYNA ..... 36

5.1.2. General Steps of Finite Element Analysis of Sheet Metal Forming ..... 36

5.2. Numerical Modelling ..... 36

5.3. Mesh ..... 37

5.3.1. Mesh Sensitivity ..... 39

5.4. Element Formulation ..... 40

5.5. Contact ..... 40

5.6. Tool Motion ..... 40

5.7. Gas Spring Force ..... 41
5.8. Outputs & Solver Options ..... 42
5.9. Springback ..... 43

CHAPTER 6. RESULT AND DISCUSSIONS ..... 44
6.1. Sheet Metal Forming Results ..... 44
6.2. FEA Results ..... 47
6.3. Validation of Numerical Approach ..... 55
6.4. Forming Limit Diagram ..... 59
6.5. Process Optimization Study ..... 61

CHAPTER 7. CONCLUSION ..... 65

REFERENCES ..... 69

# LIST OF THE FIGURES

**Figure** **Page**

Figure 1. Greenstar 2000 Combi Boiler ..... 1
Figure 2. Illustration of the combi boiler installation in house ..... 2
Figure 3. Schematic of Central Heating Mode ..... 3
Figure 4. Schematic of Domestic Hot Water Mode ..... 4
Figure 5. Detailed view of the plate heat exchanger ..... 5
Figure 6. Copper foil (filler material) between two stainless steel channel plates ..... 6
Figure 7. Finite element model of bulge test (a) and applied hydraulic pressure (b) ..... 8
Figure 8. Yield surfaces for the AA6016 T4 aluminum alloy ..... 9
Figure 9. Experimental tensile stress–strain curves of AISI 304L steel at quasi-static and high strain rates and corresponding Johnson–Cook model fits. ..... 11
Figure 10. Experimentally and numerically deformed pictures of study ..... 11
Figure 11. Schematic representation of stretching setup ..... 12
Figure 12. Illustration of the basic forming setup ..... 14
Figure 13. 4 Stage of the plate production ..... 15
Figure 14. PHE Plate (a) and filler material (b) ..... 15
Figure 15. Direction of the sheet metal ..... 17
Figure 16. True stress-strain curves of 316L stainless steel at different strain rates ..... 19
Figure 17. Springback effect after forming operation ..... 20
Figure 18. Shimadzu Tensile Test Machine ..... 21
Figure 19. Standard tensile test sample ..... 22
Figure 20. Uniaxial tensile test result of the 316L stainless steel with different degree ..... 24
Figure 21. Uniaxial tensile test result of the 304 stainless steel with different degree ..... 24
Figure 22. Gerhard Gutscher’s design of a bulge test ..... 25
Figure 23. Hydraulic bulge test results of the 316L and 304 stainless steel ..... 26

**Figure** **Page**

Figure 24. Nakajima Test Setup & Samples ..... 27
Figure 25. Flow limit diagram of the 316L stainless steel ..... 27
Figure 26. Split Hopkinson tension bar schematic ..... 28
Figure 27. Split Hopkinson Tension Bar ..... 29
Figure 28. DIC image of the sample ..... 30
Figure 29.SHPB test results of the 316L and 304 stainless steel ..... 30
Figure 30. Numerical Tensile Test Results for 0/45/90 degree rolling directions and average with *MAT133_BARLAT_YLD2000 ..... 32
Figure 31. Comparison of numerical and experimental tensile test stress-strain results ..... 32
Figure 32. Comparison of numerical and experimental hydraulic bulge test stress-strain results ..... 33
Figure 33. MAT_BARLAT_YLD2000 parameters in Ls-Dyna ..... 34
Figure 34. CAD Data vs. Simplified Model ..... 37
Figure 35. Blank (a), Punch (b), Blankholder (c), Die (d) ..... 38
Figure 36. Aspect ratio and time step size of the blank ..... 38
Figure 37. Mesh sensitivity outputs regarding to different mesh sizes ..... 39
Figure 38. Applied load and velocity for tools ..... 41
Figure 39.Segment set for gas spring loads ..... 41
Figure 40. Characteristic Load Curve for Gas Springs ..... 42
Figure 41. Gas Spring and Technical Details ..... 42
Figure 42. Scanning results of PHE plate ..... 44
Figure 43. Cross section of the PHE plate along the y-axis from middle of the plate ..... 45
Figure 44. Cross section of the PHE plate along the x-axis from middle of the plate ..... 45
Figure 45. XRD Measurment Points ..... 47
Figure 46. Effective stress of 316L stainless steel PHE plate ..... 48
Figure 47. Effective stress of 304 stainless steel PHE plate ..... 48
Figure 48. Residual stress of 316L stainless steel PHE plate ..... 49
Figure 49.Residual stress of 304 stainless steel PHE plate ..... 49
Figure 50. Effective plastic strain of 316L stainless steel PHE plate ..... 50
Figure 51. Effective plastic strain of 304 stainless steel PHE plate ..... 50

**Figure** **Page**

Figure 52. Shell thickness distribution of 316L stainless steel PHE plate ..... 51
Figure 53. Shell thickness distribution of 304 stainless steel PHE plate ..... 51
Figure 54. Critical thickness reduction areas of PHE plate ..... 52
Figure 55. Comparison of the thickness reduction ratios of 316l & 304 stainless steel ..... 52
Figure 56. Plate cross-section along y-axis ..... 53
Figure 57. 316L stainless steel z-displacement along y-axis from A to B ..... 53
Figure 58. 304 stainless steel z-displacement along y-axis from A to B ..... 53
Figure 59. Comparison of 316L&304 z-displacement along y-axis from A to B ..... 53
Figure 60. Plate cross-section along x-axis ..... 54
Figure 61. 316L stainless steel z-displacement along x-axis from C to D ..... 54
Figure 62. 304 stainless steel z-displacement along x-axis from C to D ..... 55
Figure 63. Comparison of 316L & 304 stainless steel z-displacement along x-axis from C to D ..... 55
Figure 64. Cross section along the x axis comparison between 3D scanned part and FEA result for 316L, a- General View, b- Detailed View ..... 56
Figure 65. Cross section along the y axis comparison between 3D scanned part and FEA result for 316L, a- General View, b- Detailed View ..... 57
Figure 66. Numerical results of the plate according to FLD curve ..... 59
Figure 67. Wrinkles area on the plate ..... 59
Figure 68. Element-base major minor strain of the plate for 316 L Stainless Steel in FLD ..... 60
Figure 69. Max effective stress graph of PHE according to x-times punch velocity ..... 62
Figure 70. Max plastic strain graph of PHE according to x-times punch velocity ..... 63
Figure 71. Cross section along the y axis comparison between x-times punch velocities for 316L ..... 64

# LIST OF TABLES

**Table** **Page**

Table 1. Young's Modulus [GPa] of the 316L and 304 stainless steel ..... 23
Table 2. Yield Strength [MPa] of the 316L and 304 stainless steel ..... 23
Table 3. Lankford Parameters of the 316L and 304 stainless steel ..... 23
Table 4. Biaxial yield strength of the 316L and 304 stainless steel..... 26
Table 5. Biaxial Lankford parameters of the 316L and 304 stainless steel ..... 26
Table 6. Material properties of the bar used in SHTB ..... 29
Table 7. Cowper-Symonds C and P parameters of 304 & 316L Stainless Steel ..... 30
Table 8. Material parameters from the characterization test of the 316L & 304 stainless steel ..... 31
Table 9. Solution time according to mesh sizes..... 39
Table 10. XRD Measurement Result ..... 46
Table 11. Maximum Effective Stress Values of PHE Plates ..... 48
Table 12. Residual stress of stainless steel PHE plates ..... 49
Table 13. Maximum effective plastic strain values of PHE plates ..... 50
Table 14. FEA Results of Residual Stresses for XRD Measurement Points ..... 58
Table 15. Comparison between XRD Measurement Results and FEA Results ..... 58
Table 16. Results from FLD curve ..... 61
Table 17. Tabular results of thickness reduction in three different regions (Valley, Hill, Hole) according to x-times punch velocity [33] ..... 62

# CHAPTER 1

# INTRODUCTION

The need for heating has been one of the basic needs throughout human history. Humanity has used different heating systems together with technology and maintained its life throughout history. Today, both energy efficiency regulations and global energy crises have increased expectations on heating and air conditioning systems. As a result of these experiences, companies continue to work to meet the needs of their customers with devices and systems with maximum efficiency with technological innovations. Combi boilers shown in figure 1 are one of these heating systems. The heat exchanger, which is the subject of this study, is an important component for combi boilers and offers an efficient solution to meet the needs of customers.

Figure 1. Greenstar 2000 Combi Boiler
(Source: Worcester Bosch, 2023)

Combi boilers are compact air-conditioning devices designed to meet the hot water and heating needs of the environment in which they are used. During its operation, it usually heats water using natural gas (hydrogen, or other heat sources) as an energy source. Heated water can be used for two purposes. It heats the environment by circulating in the radiators in a closed loop (Figure 2), or the water heated in the primary heat exchanger meets the domestic water in the secondary heat exchanger and meets the hot water need of the user.

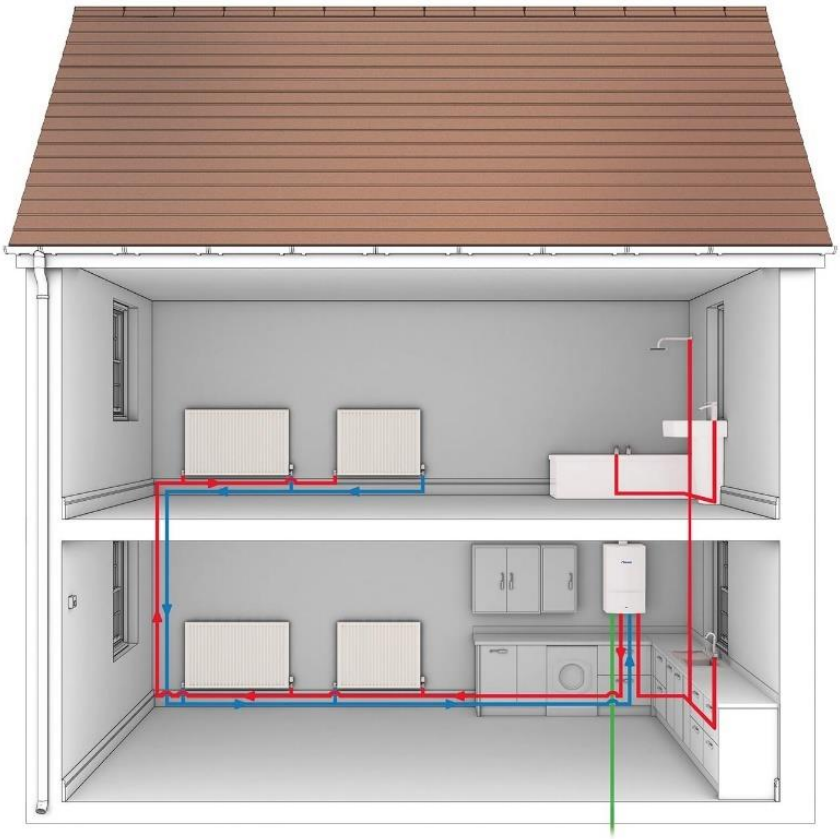

Figure 2. Illustration of the combi boiler installation in house
(Source: Worcester Bosch, 2023)

There are two different modes in combi boilers. Central heating (CH) shown in figure 3 is a closed loop. The purpose of this mode is to heat the environment and meet the user's warming needs. The gas in the primary heat exchanger burns and heats the water in it. Due to the three-way valve being in the closed position, the hot water in it passes directly to the radiators and heats the environment. In order to regain the heat lost during the heating of the environment, the primary light returns to the heat exchanger by means of the pump and continues the cycle in a reheated manner.

Domestic hot water (DHW) mode shown in figure 4 is activated when the user needs hot water. In Domestic Hot Water mode, again water heated in the primary heat exchanger. The water heated in the primary heat exchanger is directed to the secondary heat exchanger by the three-way valve instead of going to the radiators. Then heated water come together with the cold water coming from the mains (which is called domestic water) in the secondary heat exchanger which is PHE. Heat is transferred hot to cold water and hot water. The domestic water heated here is used for the hot water needs of the user. The plate heat exchanger, which is the subject of the thesis, is used in this mode.

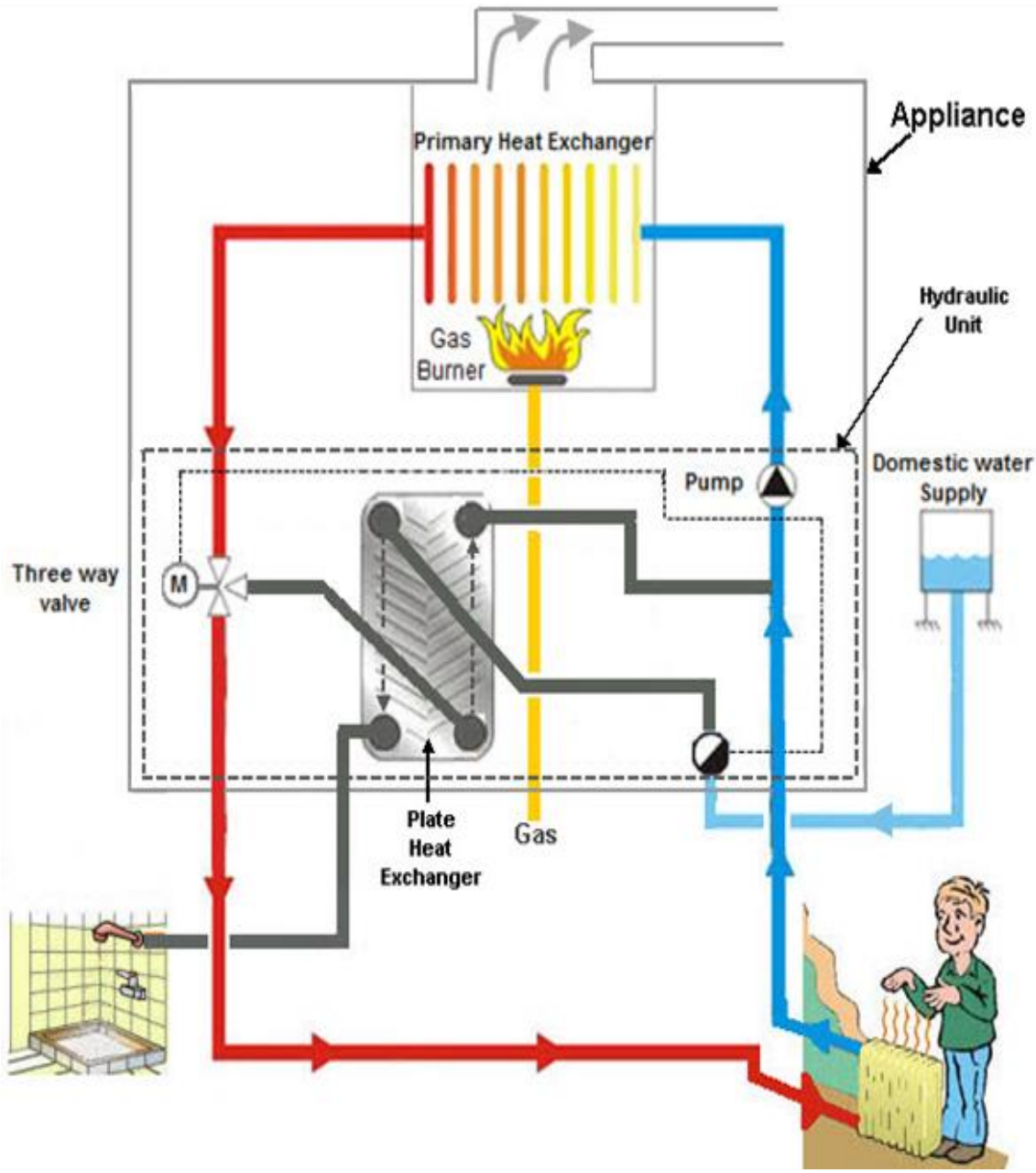


Figure 3. Schematic of Central Heating Mode

(Source: Gürler, Y., 2018)

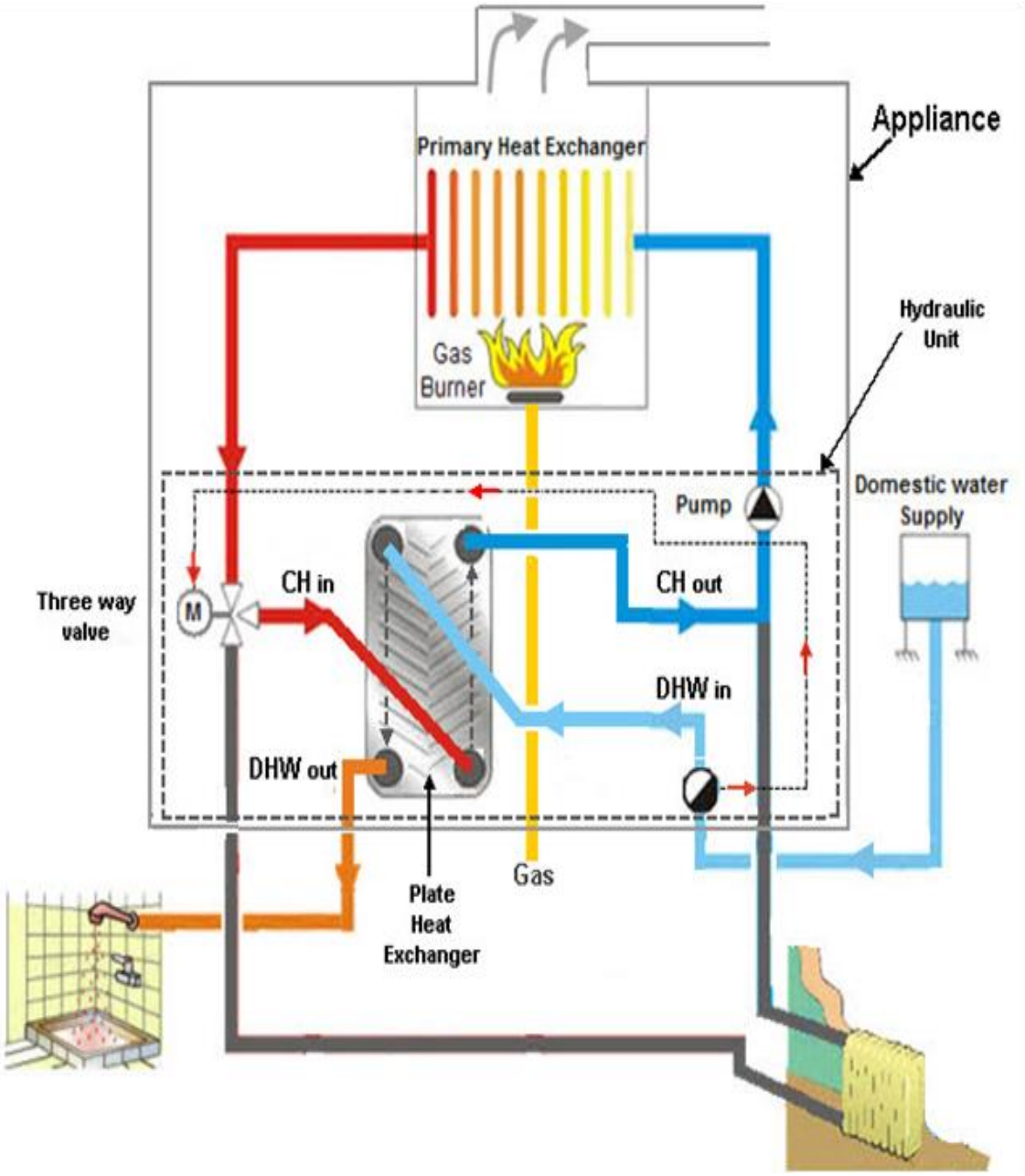


Figure 4. Schematic of Domestic Hot Water Mode

(Source: Gürler, Y., 2018)

Plate heat exchangers are used in many industries due to their compact size and thermal efficiency. Plate heat exchangers have a very important place in the air conditioning industry. Plate heat exchangers are a component that performs heat transfer between two or more fluids. They can have designs in various sizes and shapes according to their usage areas.

The plate heat exchanger used in this study is corrugated type. Component design and reliability affect system performance during the plate heat exchanger development process.[7] In the component that is the subject of the thesis, 80 C water coming from CH water transfers heat to the water coming from domestic cold water (DCW) without any contact between fluids. As a result of heat transfer, domestic hot water has a temperature of around 60 C.

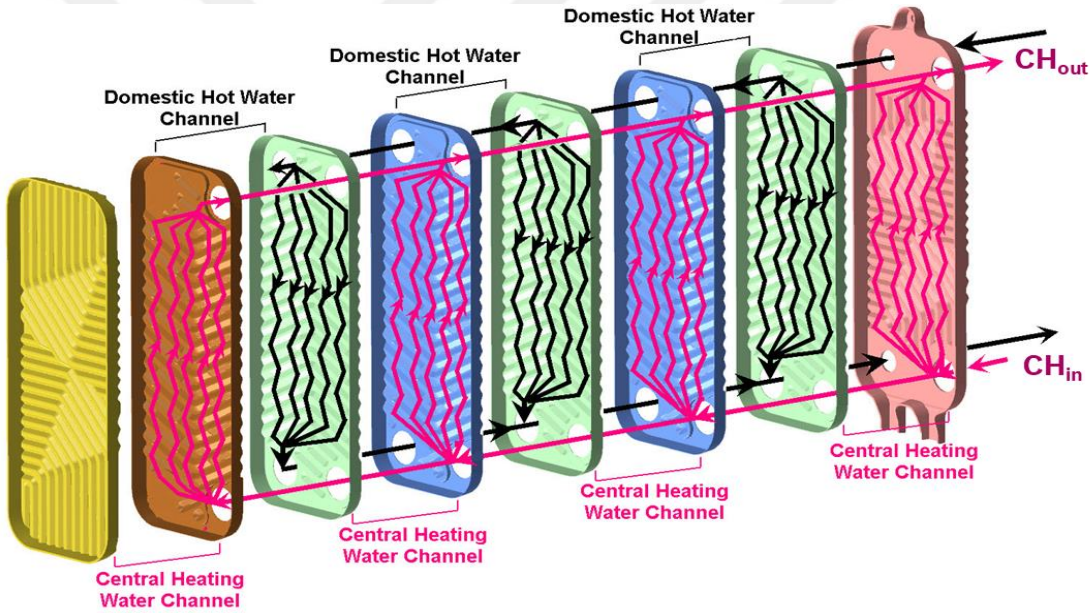


Figure 5. Detailed view of the plate heat exchanger

(Source: Gürler, Y., 2018)

The plates that make up the plate heat exchanger are connected to each other by brazing. In current production, it is produced from 316L stainless steel with PHE plate. Copper material is used as brazing filling material. Copper has a high wetting ability with steels and is also corrosion resistant. PHE plate and filler material have the same pattern. The reason for this is that two different material rolls are exposed to the forming operation at the same time during production and form the same pattern.

Subsequently, the PHE plates and filler materials formed are stacked on top of each other to form PHE, as seen in Fig. The number of plates to be used in PHE may vary depending on the device to be used. The plates stacked on top of each other are sent to the vacuum brazing furnace after a small compression operation. The PHEs, which are heated in this furnace at a certain temperature and hour, complete the process by melting the copper in the vacuum environment and filling the brazing cavities. The PHEs removed from the vacuum brazing furnace become suitable for mounting on appliances.

Figure 6. Copper foil (filler material) between two stainless steel channel plates (Source: Hayta, Y., 2020)

## 1.1. Problem Definition and Aim of the Study

The main intension of this thesis is to investigate the effect of the process parameters of the sheet metal forming method on the formability of the stainless-steel corrugated plates. That are being used in brazed plate heat exchangers (PHE). This study will be used in the ratio and innovation activities to be carried out under current conditions. When any material changes or pattern change is planned on PHE plates, the forming performance of the plate can be examined based on personal experience and by producing a sample mold. Thanks to this study, money, and time to be spent on mold manufacturing before sample production will be saved. The changes to be made will first be tested in the simulation environment and molds will be produced for designs and materials with satisfactory results and forming process will be carried out.

The first step to develop a reliable simulation methodology is to make the correct material characterization and create a material model. In this context, the results of both outsourced and conducted tests were compiled throughout the study. In order to adapt the test data obtained to the material model in the most appropriate way and to reflect the

property of the material, an anisotropic and strain rate sensitive material model was developed. In the first step of the study, a material model was developed with the data obtained from the tests and verified with the numerical models of the material tests.

Then, the forming process was analyzed. There are several process parameters that effects the formability of the corrugated plates such as punch velocity, gas spring force, lubricant/friction. However, it has been thought that the punch velocity and gas spring force are more important among the others. Therefore, the focus will be on these parameters during the numerical studies. Determining the forming process parameters will also be done in this study. The displacement-time curve for punch velocity will be determined with a high-speed camera, and characteristic curves will be extracted for gas spring force. Obtaining these parameters is also important because of the increase in process know-how. On the other hand, the effect of the material changes from 316 L to 304, skirt angle on the formability was investigated as well.

During this study, Ls-Dyna to be used as numerical simulation tool. Ls-Dyna gives effective results in explicit forming simulations thanks to its capability. Digitization of the manufacturing process will offer the chance to observe known and unknown effects/results about the process. Simulation will be used in order to transfer know-how about the process in the digitalized world. For the numerical investigation of formability behavior of the corrugated plates, material modelling is carrying crucial importance. In order to reflect the property of the material to the simulation in the most accurate way, a material model determination study was carried out [9] The anisotropic structure of the sheet metal and the strain rate sensitivity were taken into consideration and the material card selection was made accordingly. Therefore, it is intended to use BARLAT's material model by including the strain rate effects. As a result of these numerical investigations the formability index was evaluated by considering; thickness reduction, springback (warpage), residual stresses etc.

Having a validated numerical model and methodology makes it possible to observe the effect of material, process and pattern on the plane. Different materials or patterns can be used to increase the heat transfer capability of the plate type heat exchanger. After the validated numerical model, different material types, different process parameters, and different patterns on the plate can be studied more easily than it is now. This methodology saves money and time in the development process of the plate heat exchanger.

# CHAPTER 2

# LITERATURE

Recent studies in the literature on sheet metal forming process simulation methodology are examined in this section. Studies on the numerical analysis of sheet metal forming have been going on since the 1960s.

## 2.1. Literature Survey

Maker B. N. And Zhu X. [10] has prepared a guideline publication for those who are familiar with numerical programs and want to make sheet metal forming simulations in this numerical modeling program. The publication they have prepared contains detailed information about the numerical parameters to be considered in the setup of the metal forming simulation setup in the Ls-Dyna program and the selection of these parameters. In another publication[11] they prepared, details about springback analysis after forming simulation were also included.

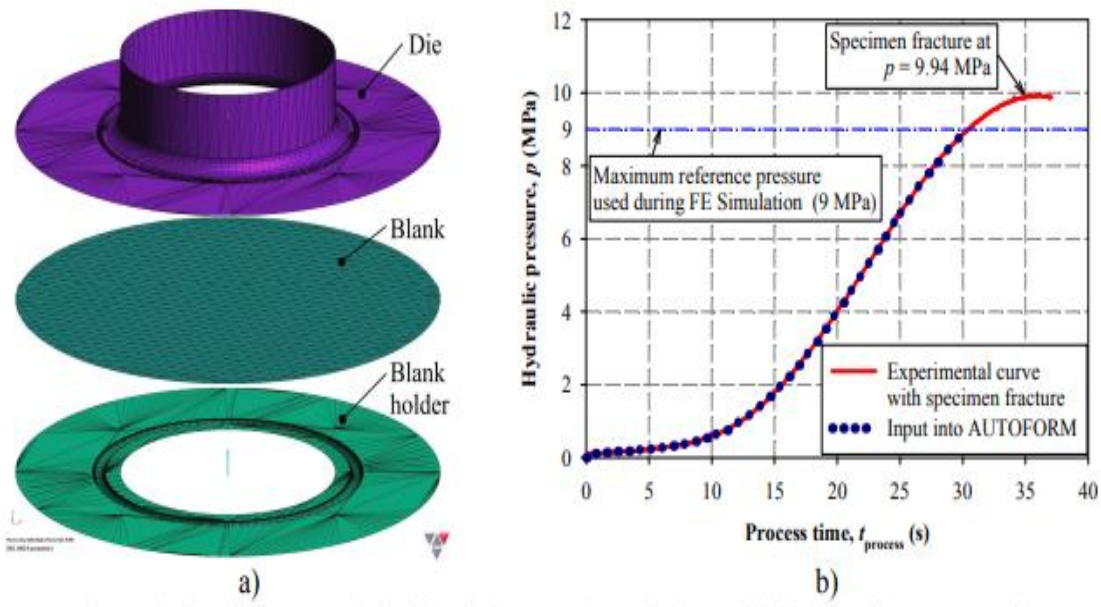


Figure 7. Finite element model of bulge test (a) and applied hydraulic pressure (b) (Source: Lazarescu, L., 2013)

Lazarescu, Lucian, et. al., [12] have studies on the effect of mechanical parameters used as inputs during material modeling on the simulation of the sheet metal forming process. In this study, the differences between the Hill-48 yield criterion, the Barlat-89 yield criterion and the BBC 2005 yield criterion have been examined. For comparison, they set up a hydraulic bulge test setup. They compared the accuracy of three different yield criteria over thickness and strain distribution. As a result, they concluded that the BBC 2005 yield criterion is more accurate for the material used in the study shown in figure 7.

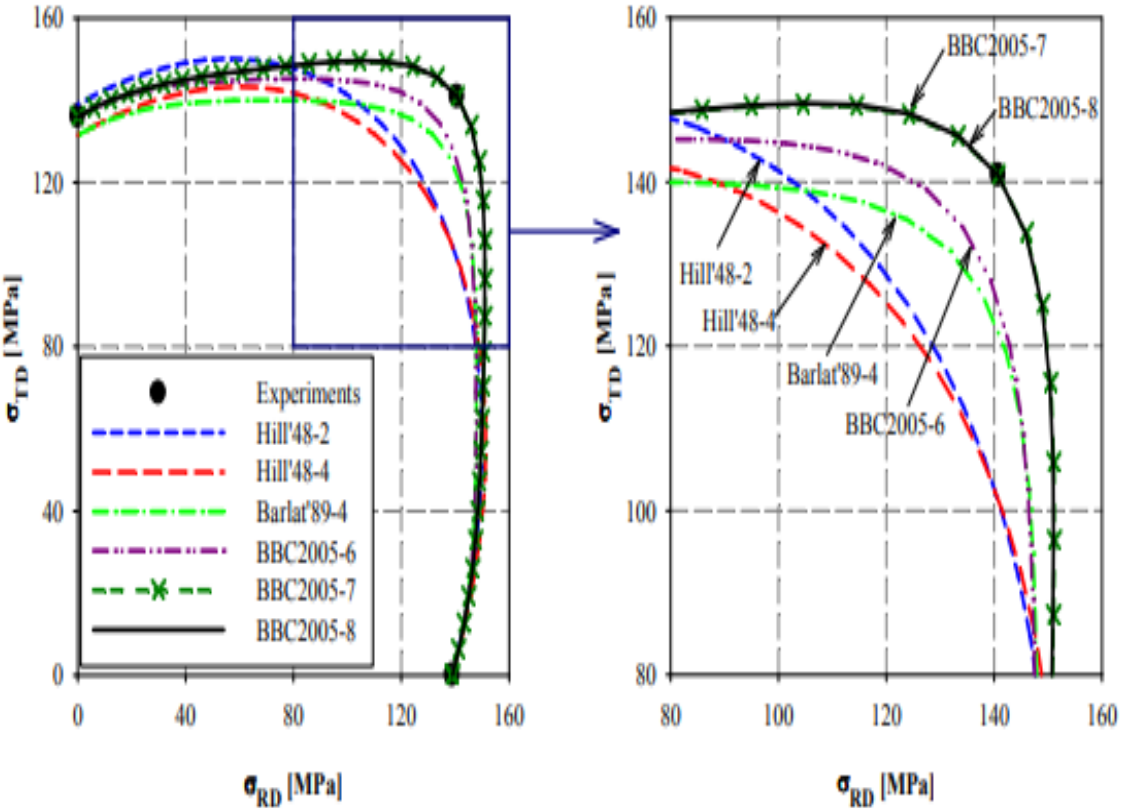


Figure 8. Yield surfaces for the AA6016 T4 aluminum alloy

(Source: Lazarescu, L. et. al, 2013)

Banabic, D., et al. [13] conducted a study on the effect of the material model on the results in sheet metal forming simulations. As a result of this study, they mentioned the importance of the parameters to be considered in the material model for a sheet metal forming simulation with high precision. As output, they said that uniaxial yield stresses

and r-values are important. In addition, they emphasized the importance of including biaxial yield stress values in the model in terms of model precision.

Deng, Z., et al., [14] examined the effect of the material model on the sheet metal forming production in their study. In this context, they carried out tests for AA 6016 Al alloy material and determined the anistropic property of the material. In the study, 4 different strain hardening models and 3 different yield criteria were examined. As a result, they determined that the combination of BBC2005 yield criterion and Swith-Hocket Sherby strain hardening model together gave the most accurate results for their materials.

Sener, B., et al., [15] also investigated the effect of the material model on the sheet metal forming production and the anisotropic behavior of the material in their study. In this context, uniaxial and biaxial tests were carried out for the AISI 304 stainless steel material, and they determined the anisotropic property of the material. They chose the fourth-order polynomial yield criterion as the material model and implemented it to the numerical model as user-defined. As a result of their work, they proved the effectiveness of the material model they created and validated it.

Noren M. [16] carried out a sheet metal forming process simulation in order to understand and optimize the deformation mechanism that occurs during the production of plate type heat exchangers with his thesis. As a result of the study, it was studied to increase the existing knowledge and to optimize the design of the produced plate. The results of the two different simulation models prepared are as follows; While the simulation prepared with the current design for model validation gives realistic results, there are deviations in the results in the simulations made for design improvement.

Tasdemirci, A., et al., [17] in their study were created the model of sheet metal with the deep drawing method shown in figure 10, and then examined the behavior of the sample they produced with the forming method under static and dynamic loads. In the study, strain-rate sensitivity of AISI 304L steel (figure 9) and its effects on crushing were investigated.

Sigvant, M., et al[18] mentioned that another factor that increases the quality of the sheet metal forming process simulations is the tribology and friction pattern between the workpieces. They stated that the common friction model is used in many models in the literature, and they examined the friction issue in detail. In addition, they examined the effect of strain rate sensitivity during forming. They emphasized the effect of friction model on the strain rate sensitivity feature of the material.

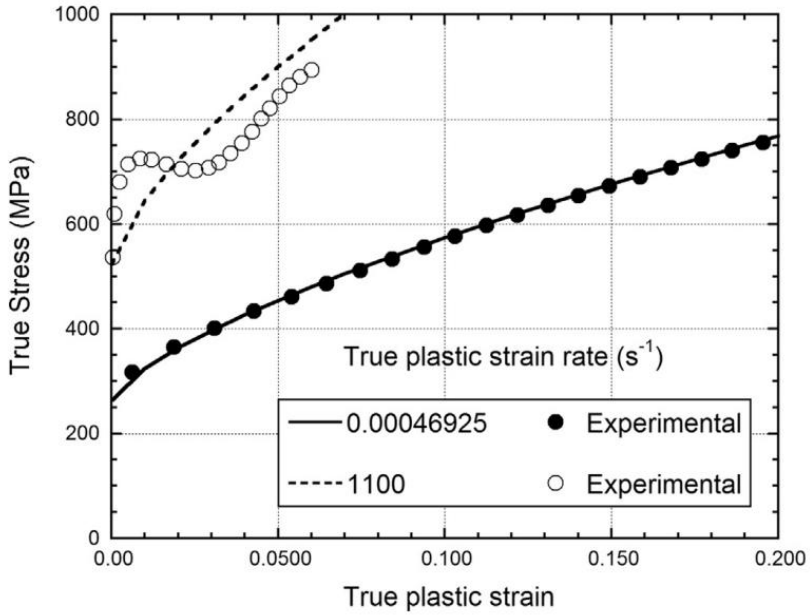


Figure 9. Experimental tensile stress–strain curves of AISI 304L steel at quasi-static and high strain rates and corresponding Johnson–Cook model fits. (Source: Sener, B. et. al, 2020)

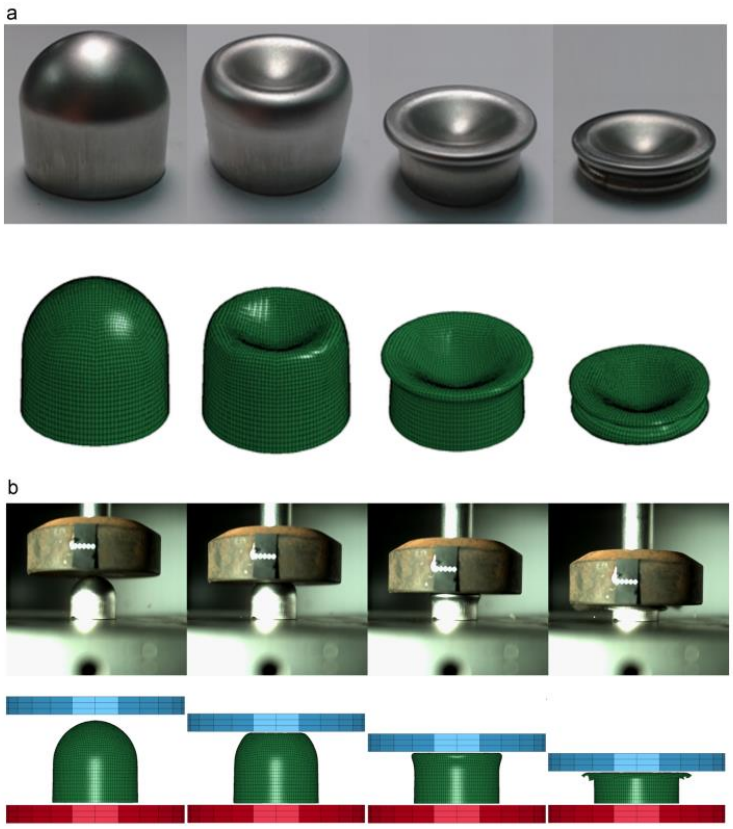


Figure 10. Experimentally and numerically deformed pictures of study (Source: Tasdemirci, A., et al., 2015)

The deformation that occurs in metals after the sheet metal forming process is called springback. In this context, Lee, S. W., et. al.,[19] examined the effect of numerical parameters on springback estimation and determined and compared numerical analysis parameters such as element size, punch speed, contact parameters. Optimum parameters were selected together with the experimental studies. Panthi, S. K., et. al., [20] on the other hand, examined the design parameters and material properties of sheet metal and the effects of lubricant use on the springback estimation. The studies have been validated experimentally and numerically.

Pham, Quoc Tuan, et. al., [21] have worked on the springback prediction for the Al 7000 series materials, which are frequently used in the aerospace industries. In this study, experimental and numerical modeling activities were carried out in parallel. As a result, it is emphasized that material properties, material model and numerical parameters are important for springback prediction as in previous studies.

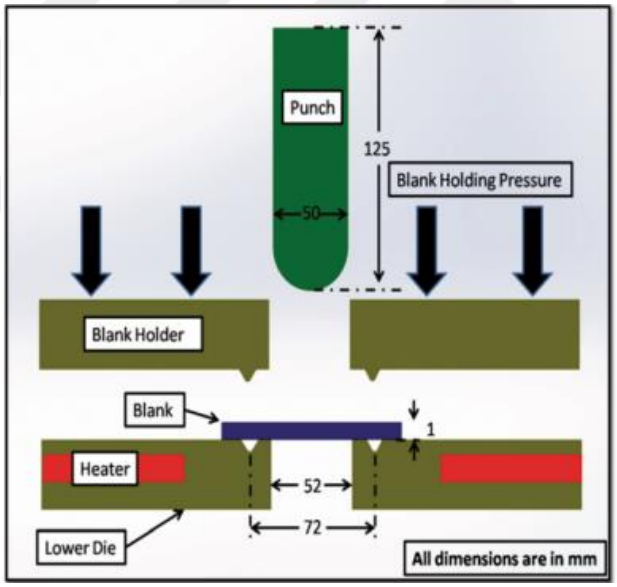


Figure 11. Schematic representation of stretching setup
(Source: Dharavath, B., et. al., 2020)

Dharavath, B., et. al., [22] investigated ASS 316L stainless steel in their study test setup shown in figure 11. They completed the selection of the material model to be used in the hot forming operation of the ASS 316L material and made a comparison between the Johnson Cook and Modified Zerilli-Armstrong material models. As a result, they determined that the modified Zerilli-Armstrong material model gave a more accurate

result. They also created a theoretical forming limit diagram using the Marciniak-Kuczynski model. The studies were compared experimentally and numerically. The working range of the material used in this study is between 750 C - 900 C.

Park, Namsu, et. al., [23] conducted a study to predict the forming performance and sudden fracture formation of metal materials using a fracture-based forming limit diagram. The fracture based anisotropic yield criterion they use is Lou-Huh fracture criterion modified from Hill's 48. As a result of the study, it has been determined that the most suitable fracture forming diagram for high strength steel plates is based on polar effective plastic strain.

Pilthammar, J., et. al., [24] have elastically modeled tools that are generally assumed and modeled as rigid in their numerical modeling activities. The reason for this is that they want to obtain more accurate results in models in some cases according to the demands of the production. For this reason, the type of press, tool design, and material of the workpiece should be considered in choosing this assumption. Within the scope of the study, a comparison of rigid and elastic tool usage was made in numerical analyzes and as a result, they observed that the use of elastic tool in modeling gave more consistent results.

# CHAPTER 3

# THEORY

Sheet metal forming, as in many production processes, is a production process used to create a complex geometry of raw material, size, tolerance, and appearance. In the sheet metal forming process, blank materials can be formed into complex shapes with the help of molds. The shaping mechanism during this process is plastic deformation. On the blank material during the process, there is no extreme thinning and no deterioration in surface roughness. Single-sided or double-sided (punch and die) molds are available. Making the design by considering the springback effect during the mold design is related to how much the material will resemble the final shape desired. Sheet metal forming operations are generally cold forming methods.[30]

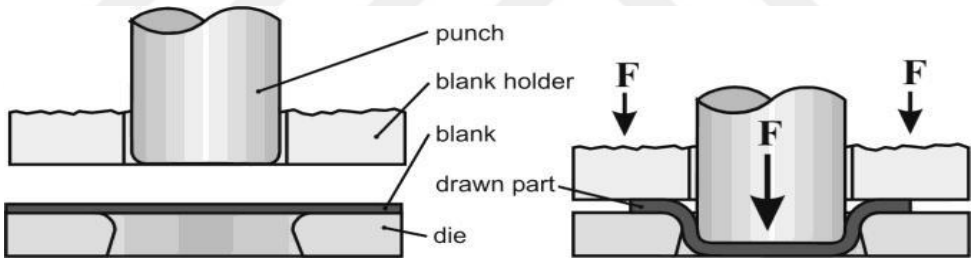


Figure 12. Illustration of the basic forming setup
(Source: Groche, P., et. al, 2004)

Plate heat exchanger is produced from sheet metal and the process is completed in 4 steps. The first two of these operations are cutting, the third is shaping, and the last is drilling. There are 3 important process parameters in the forming process. The first is the punch speed, the second is the gas spring force, and the last is the friction between the components. While doing the numerical modeling of this process, first the characteristic curves of the gas spring forces were examined, then the displacement-time curve of the punch was created using a high-speed camera. Literature was used for the coefficient of friction. The picture below (figure.14) shows the plate produced as a result of the manufacturing process.

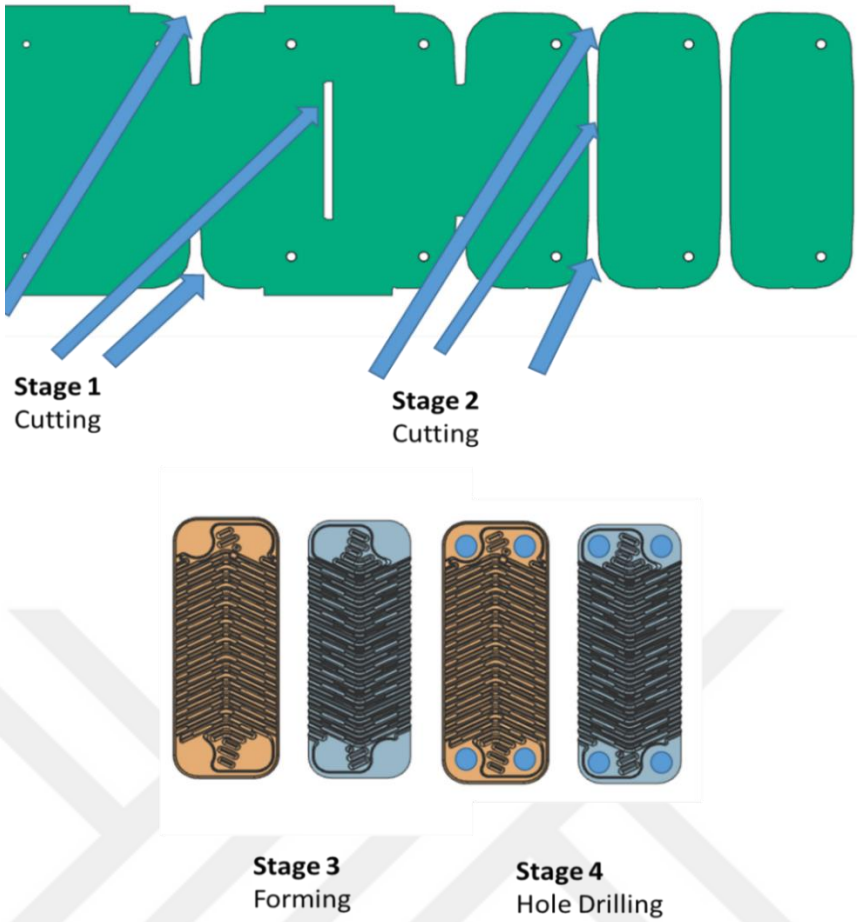


Figure 13. 4 Stage of the plate production

(Source:Gürler, Y., 2018)

Figure 14. PHE Plate (a) and filler material (b)

(Source: Hayta, Y., 2020)

The stress-strain curve is a fundamental curve that helps to understand the properties of the material. The test used to obtain the stress-strain curve is called the uniaxial tensile test. By using the uniaxial tensile test and results, a lot of information about the stress-strain curve is obtained. The information obtained is such as Elastic Modulus, Yield Strength, Ultimate Tensile Strength, Failure Strain values. Another issue to be examined in the stress-strain relationship is engineering and true stress-strain curves and the difference between them which starts after yielding.

The engineering stress-strain curve obtains the stress value by dividing the force exerted on the specimen during the test by the initial cross-sectional area of the specimen. It is assumed that there is no change in the cross-sectional area of the sample during uniaxial tensile test.

The true stress-strain curve, unlike the engineering stress-strain curve, considers the change in the cross section of the sample when calculating. Engineering stress-strain values are used to calculate the true stress-strain. A transformation is performed between engineering and true in accordance with the principle of constant volume change. The equations below show true stress and true strain calculations from engineering.

$$S = \frac{P}{A_0} \tag{3.1}$$

$$e = \frac{\Delta l}{l_0} \tag{3.2}$$

$$\sigma = S(1 + e) \tag{3.3}$$

$$\varepsilon = \ln\,(1 + e) \tag{3.4}$$

The stress-strain curve can be considered as two different regions. It is possible to divide the yield strength value into two as left and right. These areas are called elastic region and plastic region, respectively.

The elastic region is the area in the stress-strain curve where the relationship between stress and strain is linear. The deformation on the material in this region is not permanent. When the force acting on the material in this region is withdrawn, the material regains its original shape. It is also called the recovery region. The mechanism that occurs

in the elastic region is explained by Hooke's Law. The mathematical equations of Hook's Law are as follows:

The plastic region is the region that comes after the elastic region in the stress-strain curve, after the material passes the yield point, it enters the plastic region and undergoes permanent deformation. In the plastic region, the material undergoes deformation from the yield point to the failure point. The theory of plasticity is a more complex mathematical theorem than the theory of elasticity. It cannot be explained with a simple equation as in the theory of elasticity because there is no linear relationship between stress and strain in plasticity.[6,26]

Materials that have the same properties in all directions are called isotropic materials. In addition, materials whose properties change depending on the direction are called anisotropic shown in below figure 15. Sheet metal in many different industrial uses is also in the anisotropic material class. After the rolling process, the property of the material changes with the change in the crystallographic structure of the material, even if it is isotropic.

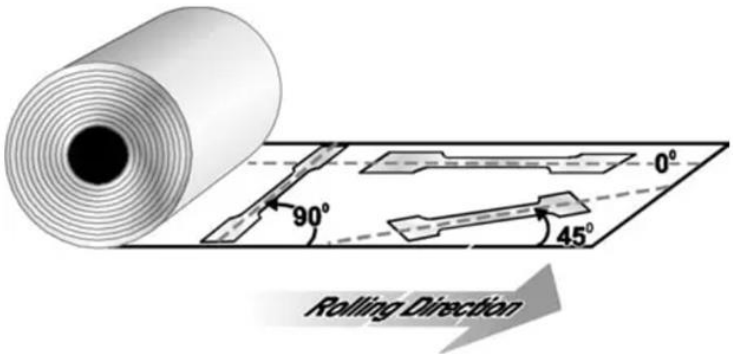


Figure 15. Direction of the sheet metal
(Source: FormingWorld, 2023)

The directional change in plastic behavior of anisotropic materials is measured by the Lankford parameter. The Lankford parameter is the directional variation coefficient of the material and can be determined with the help of uniaxial test. The Lankford parameter "r" can be expressed by the following equation.

$$r = \frac{\varepsilon_2}{\varepsilon_3} \tag{3.5}$$

where, ε1 is width strain and ε2 is thickness strain.

The tensile sample can be cut at different angles according to the rolling direction and its properties can be examined. It is possible to increase the number of measurements with different variations. One of the most common measurement methods is the measurement made from 3 different angles: rolling direction (0°), diagonal direction (45°) and transverse direction (90°). The following equation allows us to find the normal anisotropy value. The fact that the material has a different normal anisotropy coefficient compared to each other affects the thinning performance during the process. The mathematical representation of this expression is as follows. It differs according to the material type.

$$r_n = \frac{r_0 + 2.r_{45} + r_{90}}{4} \tag{3.6}$$

where,
r0, r45 and r90 are anisotropy factors, rolling direction (0°), diagonal direction (45°) and transverse direction (90°) respectively.

The measure known as Δr and referred to as "planar anisotropy" can be a positive or negative number. It is an important coefficient during material selection for the process. The smaller the Δr value of the material to be used in deep drawing processes, the more suitable it is.[28]

$$\Delta r = \frac{r_0 - 2.r_{45} + r_{90}}{4} \tag{3.7}$$

Strain rate is defined as the rate of change of the strain of the material per unit time. Materials exhibit a stable behavior against forces acting at low speeds under standard room conditions. However, the behavior of materials, such as metal forming, that undergo large plastic deformation and rapidly deform in a short time, are affected by strain-rate sensitivity. Strain-rate sensitivity is defined by the following mathematical equation and is modelled with Cowper-Symonds strain rate parameters which are C and p, in the material model.

$$\sigma_y^v(\varepsilon_p, \dot{\varepsilon}_p) = \sigma_y(\varepsilon_p)(1 + [\frac{\dot{\varepsilon}_p}{C}]^{\frac{1}{p}}) \tag{3.8}$$

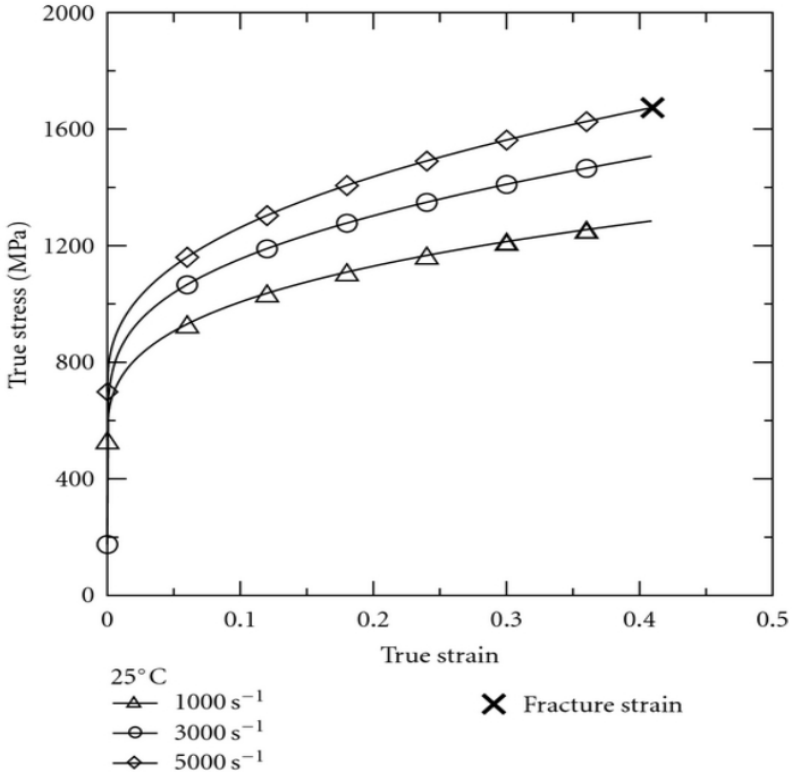


Figure 16. True stress-strain curves of 316L stainless steel at different strain rates[32]
(Source: Lee, W. S., et. al, 2011)

Springback is defined as the elastic recovery of the workpiece after the metal forming process is finished. When the workpiece is freed from the force exerted by the metal forming process, it tends to return to its original shape, starting position. With this tendency, a shape change occurs on the metal. If no improvement is made regarding this tendency in the process, the material will not come out of the mold as desired.

There are some steps that can be taken to prevent this effect. One of them is to design by considering the springback effect that may occur on the workpiece during the mold design, and the other is to add an additional step to the metal forming process, to prevent springback caused by the springback effect.[30]

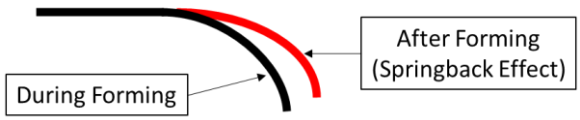


Figure 17. Springback effect after forming operation

# CHAPTER 4

# MECHANICAL CHARACTERIZATION

The purpose of this chapter is to give fundamental information about the theory of the experiments used in the study process. In this chapter, basic information about tensile test, hydraulic bulge test and Split Hopkinson tensile test performed during the study are given.

## 4.1. Uniaxial Tensile Test

The tensile test is one of the most common test methods used in material property determination. The tensile test, which is frequently encountered during engineering applications, provides access to many data from the mechanical properties of materials such as elastic modulus, yield strength, Lankford parameters, etc.

Figure 18. Shimadzu Tensile Test Machine

The test sample (Figure 19) is prepared according to certain standards. (DIN EN ISO 6892-1). There are different types of specimens that can be used during tensile testing. It should be determined in accordance with the standard according to the type of test device to be used and the connection types. The mechanical properties of the sample to be tensile tested must have the properties of the material to be determined. Sample damage caused by external factors such as extreme temperature and physical deformation should be avoided during sample preparation.

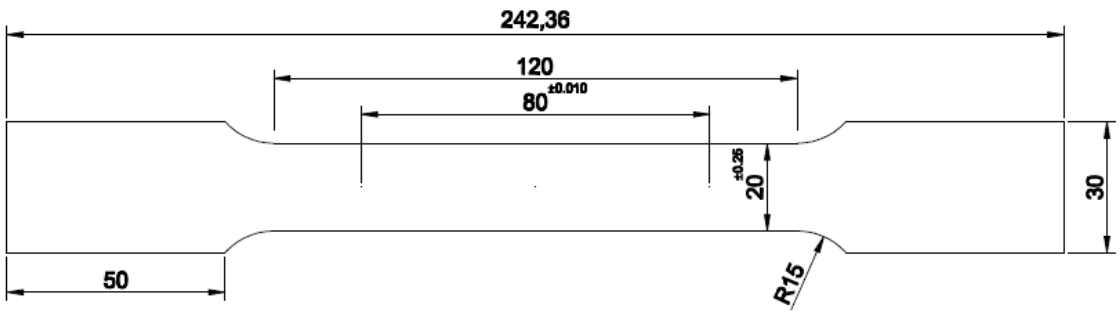


Figure 19. Standard tensile test sample

As a method, the prepared test sample is connected to the machine. At constant temperature and humidity, one side of the sample is fixed, and the other end is pulled by applying force. During this process, force-displacement data on the sample is collected. Generally, data collection is performed with the help of the extensometer. There are different types of tensile testers available today and they are classified according to the type of loading. Loading types of devices are divided into two classes as electromechanical and hydraulic. Electromechanical devices are suitable for testing at wider speed ranges. On the other hand, it is more convenient and advantageous to use hydraulic devices in situations that require more loading.

Uniaxial Tensile Test results was obtained from 5 samples each material (0°,45° and 90°). Tests Engineering Stress / Strain Curves were created in accordance with the DIN EN ISO 6892-1 standard. Repetitive tensile tests were carried out by staying within the elastic deformation limit of the material with the tensile sample prepared from the sheet material whose elasticity modulus was to be determined. Elongation during elastic loading was precisely measured using a macro extensometer.

The modulus of elasticity was determined by averaging the repeated tests. As a result of uniaxial tensile tests, stress strain curves, Young's modulus, yield strength and

Lankford parameters of the materials were obtained. The results obtained are shown in the tables and graphs below. Uniaxial tensile test tests used in this study were performed at Atılım University and fka GmbH. The material parameters obtained from the test centers are used in the material card.

Table 1. Young's Modulus [GPa] of the 316L and 304 stainless steel

| | **Young's Modulus [GPa]** | |
|---|---|---|
| | **316L** | **304** |
| 0 | 189,95 | 198,2 |
| 45 | 189,1 | 192,6 |
| 90 | 196,92 | 193,4 |

Table 2. Yield Strength [MPa] of the 316L and 304 stainless steel

| | **Yield Strength [MPa]** | |
|---|---|---|
| | **316L** | **304** |
| **0** | 302,1 | 307,0 |
| **45** | 288,1 | 285,4 |
| **90** | 294,7 | 284,0 |

Table 3. Lankford Parameters of the 316L and 304 stainless steel

| | **Lankford Parameters [r-Value]** | |
|---|---|---|
| | **316L** | **304** |
| **0** | 0,77 | 0,93 |
| **45** | 1,18 | 1,35 |
| **90** | 0,82 | 0,75 |

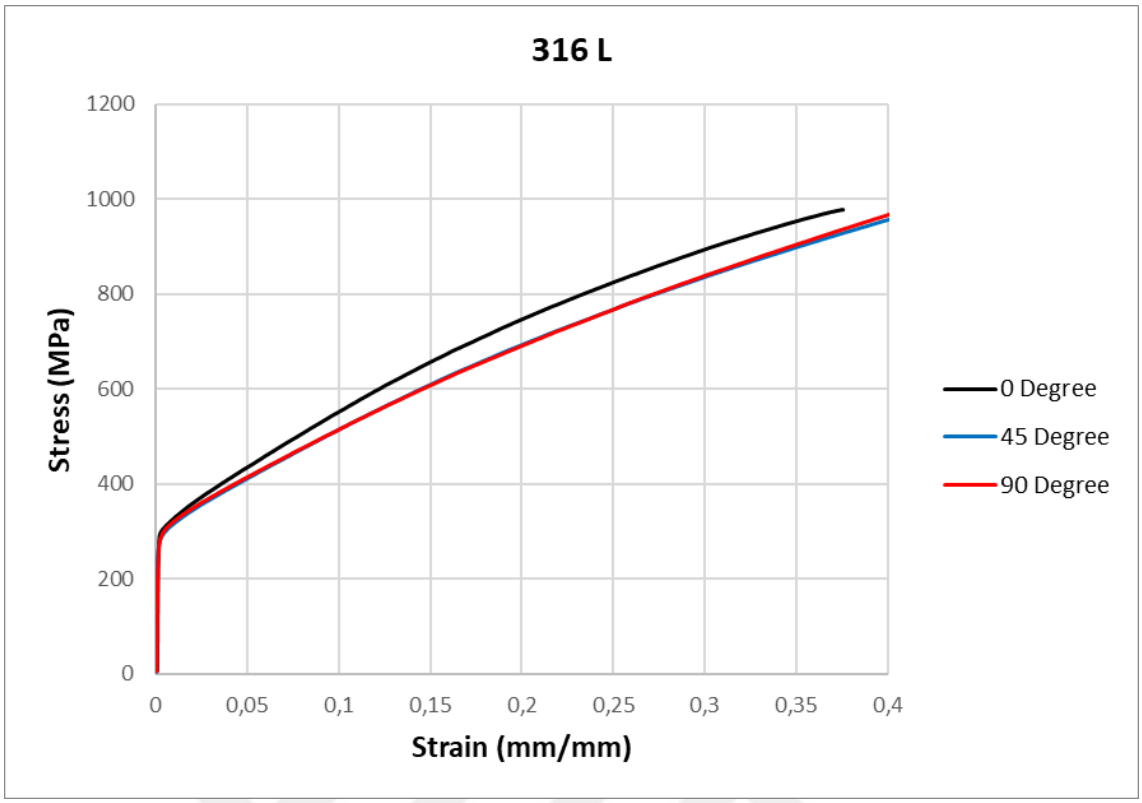


Figure 20. Uniaxial tensile test result of the 316L stainless steel with different degree

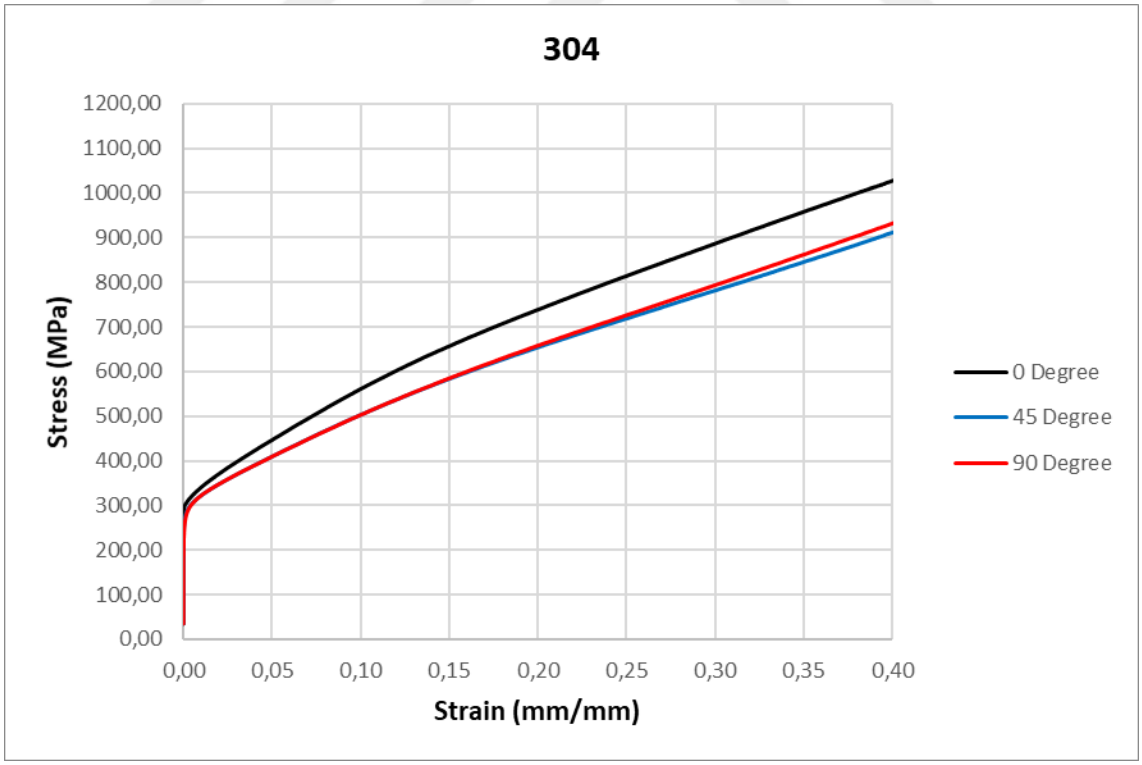


Figure 21. Uniaxial tensile test result of the 304 stainless steel with different degree

## 4.2. Hydraulic Bulge Test

The hydraulic bulge test is a method used to determine the bi-directional formability performance of sheet metals. Besides the material properties determined uniaxially by tensile test, it can be determined biaxially by hydraulic bulge test. A thin sheet sample is placed in the lower die with a cavity in its center. Then, the sheet metal sample is clamped between the upper die and the lower die. It is compressed into a compacted layer until a crack appears. A gradually increasing uniform pressure is applied to the sheet sample by pushing an incompressible liquid from the lower die cavity. With this increased pressure, the sheet sample takes the bulge form. During the forming process, thinning occurs in the apex of the sheet sample. The test results when the bulge-shaped sample bulge and bursts.

Several different test apparatus configurations are available in the literature, with varying die cavity diameter and clamping load capacity. One of the differences in bulge test designs studied in the literature is displacement measurement equipment. The displacement data required to calculate strain as a result of the test can be obtained by recording with a high-speed camera and processing with DIC in Ceok Koh's bulge test design[39], or it can be obtained by following the vertex region of the sheet sample with a position transducer in Gerhard Gutscher's bulge test design shown in figure 22.[38]

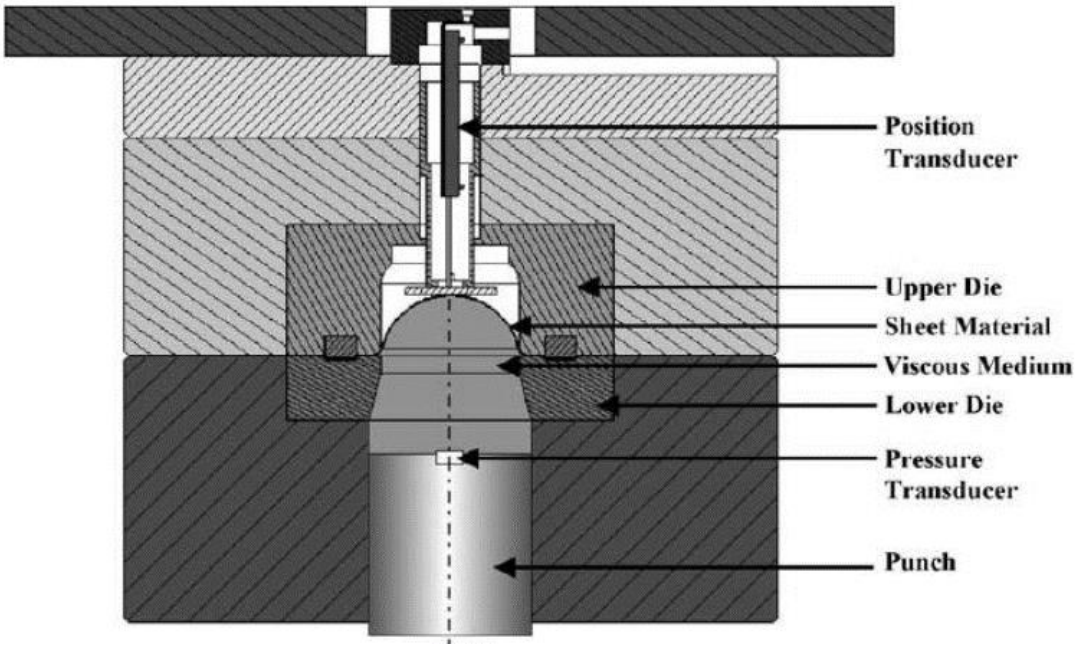


Figure 22. Gerhard Gutscher's design of a bulge test[38]

(Source: G. Gutscher, et. al, 2004)

Hydraulic bulge test results were obtained from 3 test samples for each material. Tests conducted according to DIN EN ISO 16808 standard. As a result of bulge tests, plastic stress / plastic strain curves, biaxial yield strength and biaxial Lankford parameters of the materials were obtained. Average results obtained from tests are shown in the tables and graphs below. The hydraulic bulge tests used in this study were performed at Atılım University and fka GmbH. The material parameters obtained from the test centers are used in the material card.

Table 4. Biaxial yield strength of the 316L and 304 stainless steel

| **Biaxial Yield Strength [MPa]** | |
|---|---|
| **316L** | **304** |
| 294,7 | 307,0 |

Table 5. Biaxial Lankford parameters of the 316L and 304 stainless steel

| **Biaxial Lankford Parameters [r-Value]** | |
|---|---|
| **316L** | **304** |
| 0,91 | 1,16 |

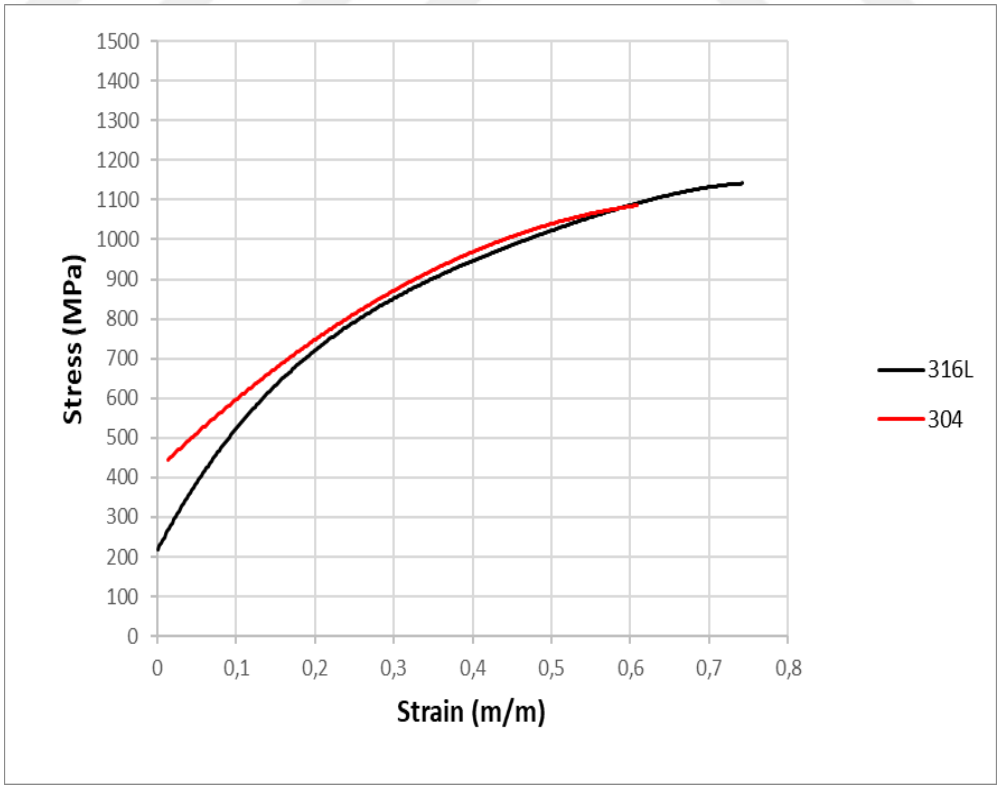


Figure 23. Hydraulic bulge test results of the 316L and 304 stainless steel

### 4.2.1. Nakajima Tests FLD (Forming Limit Diagram)

Nakajima tests were carried out on the BUP-600 Sheet Material Tester with integrated GOM-ARAMIS optical strain measurement system shown in figure 24. According to the Nakajima standard, FLC curve was obtained with 8 different strain ratio.

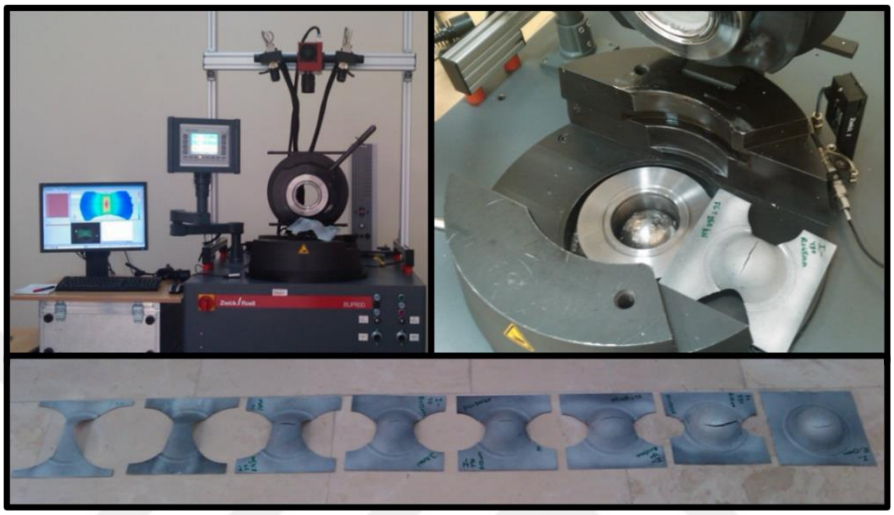

Figure 24. Nakajima Test Setup & Samples
(Source: Atılım Üniversitesi Metal Mükemmelliyet Merkezi, 2015)

Forming limit diagram of the 316L stainless steel obtained from Nakajima tests. The tests were carried out at Atılım University and the graph below was obtained for 316L stainless steel. This graph will be compared with the simulation outputs in the following sections.

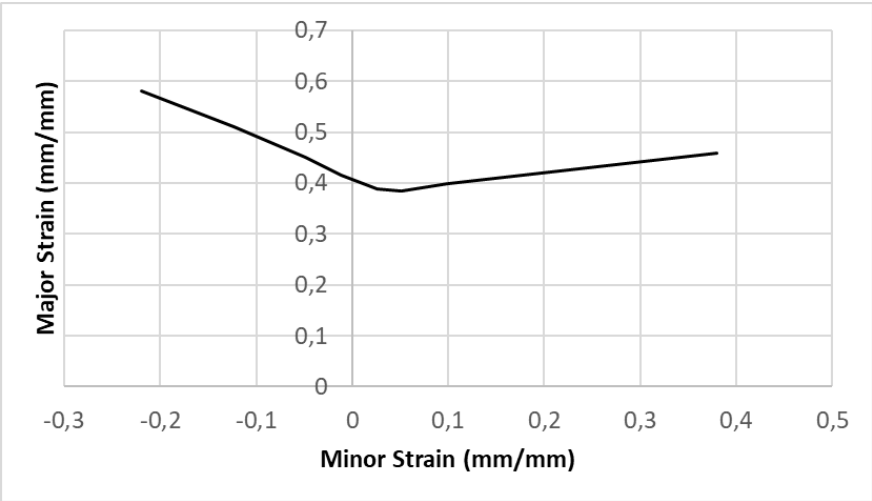


Figure 25. Flow limit diagram of the 316L stainless steel

## 4.3. Dynamic Test

Split Hopkinson Tension Bar is a test equipment (shown in figure 27) used to determine the dynamic behavior of materials. It is possible to determine the behavior of materials at different strain rates. The sample placed between the Split Hopkinson Tension Bars generates data as it ruptures.

### 4.3.1. Split Hopkinson Pressure Bar Tension Test

The basis of dynamic tensile testing is elastic wave propagation theory. The working principle is as follows: first the pressurized gas in the gas gun is released. The released gas activates the striker. Striker hits the incident bar. During this impact, a one-dimensional stress wave is generated, and the resulting stress wave propagates over the incident bar. With the help of strain gauges on the incident bar, the stress values on the bar are recorded. The wave propagated in there is called incident wave. After the incident rod, the stress wave passes to the sample, plastic deformation occurs on the sample. After this deformation, the stress wave remaining on the sample is reflected from the other end. This stress wave is also called the reflected wave. After that stage, the stress wave is transferred to the bar at the other end. The name of this bar is the transmitted bar, and the stress wave it creates is recorded as the transmitted wave.

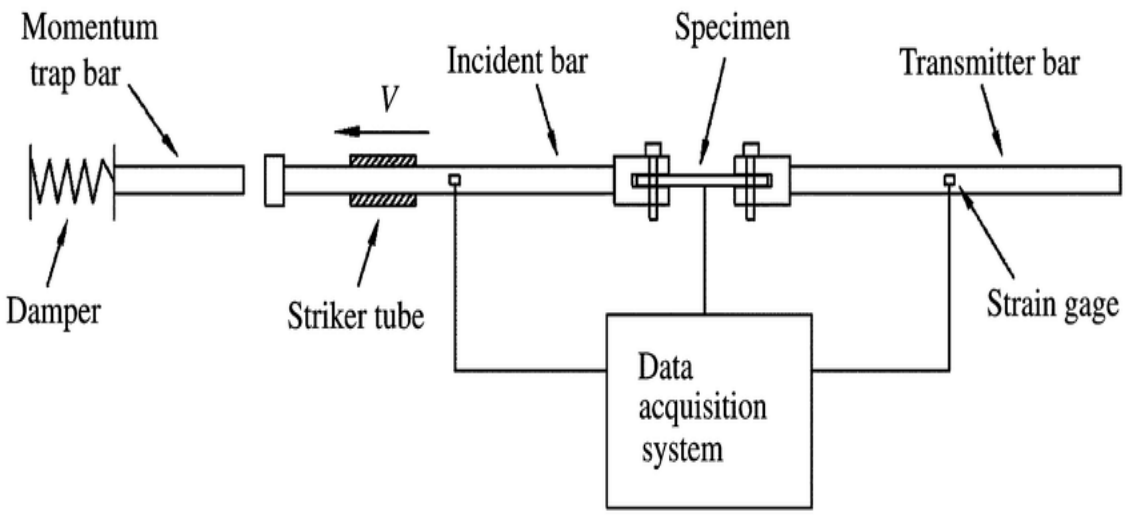


Figure 26. Split Hopkinson tension bar schematic[25]

(Source: Turan, A. K., 2018)

Figure 27. Split Hopkinson Tension Bar

The waves formed as a result of these tests are used to create the dynamic stress-strain curve of the material. During the high-speed strain test, material with the same or close properties to the tested material was used as the tool material. Also, material properties of the bar used in SHTB seen below table.

Table 6. Material properties of the bar used in SHTB

| Material | Density (kg/m3) | Elastic Modulus (GPa) | Poisson's Ratio | Yield Stregth (MPa) |
|---|---|---|---|---|
| **316 L Stainless Steel** | 8000 | 193 | 0.3 | 300 |

During the high strain rate tests, a high-speed camera was used. The sample shown in figure 28 was marked and connected to the device. Afterwards, images were recorded with 10ms time steps. The recorded images were transformed into meaningful data with the help of DIC (digital image correlation). DIC is a tracking and optical measurement method that records the change in the image. By using this method, the displacement-strain output resulting from the test is obtained. This output provides a stress-strain curve for different strain rates. Strain-rate parameters of the material is determined with using these outputs.

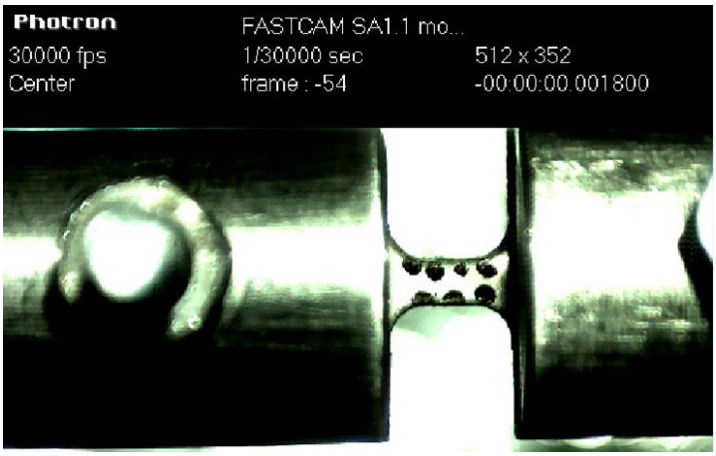


Figure 28. DIC image of the sample

Split Hopkinson test results were obtained from 3 test samples for each material. As a result of split Hopkinson tests, plastic stress / plastic strain curves at high strain-rate, strain rate parameters were determined according to split Hopkinson test results using the Cowper-Symonds constitutive equation. C and P parameters of the materials were obtained. Average results obtained from tests are shown in the tables and graphs below.

Table 7. Cowper-Symonds C and P parameters of 304 & 316L Stainless Steel

| Material | C | p |
|---|---|---|
| **316L** | 4536,2 | 2,85 |
| **304** | 1703,1 | 2,62 |

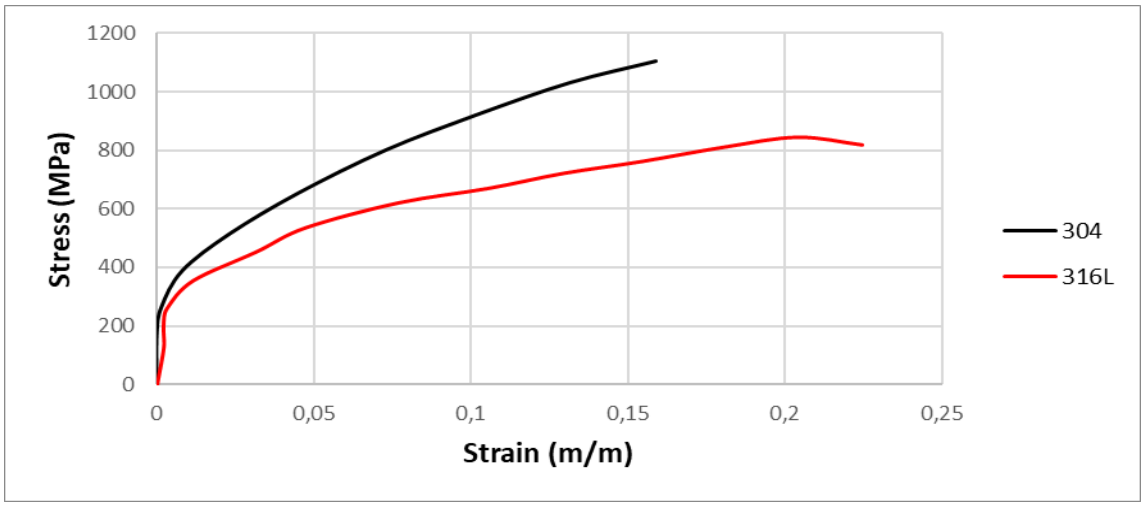


Figure 29.SHPB test results of the 316L and 304 stainless steel

As a result of material test, below parameters obtained to fulfill material cards. According to the test results, the material parameters were processed as input to the sheet metal forming process simulation to be established.

Table 8. Material parameters of the 316L & 304 stainless steel

| Material | Density (kg/m3) | Elastic Modulus (GPa) | Poisson's Ratio | Yield Stregth (MPa) | | | R0 | R45 | R90 | Rb | C | p |
|---|---|---|---|---|---|---|---|---|---|---|---|---|
| | | | | 0 Degree | 45 Degree | 90 Degree | | | | | | |
| 316 L | 7800 | 190 | 0,3 | 302,1 | 287,5 | 288,1 | 0,77 | 1,18 | 0,82 | 0,91 | 4536,2 | 2,85 |
| 304 | 7897 | 198 | 0,33 | 307,0 | 285,0 | 284,0 | 0,93 | 1,36 | 0,75 | 1,15 | 1703,1 | 2,62 |

## 4.4. Material Model

The material card has a very important place for a numerical simulation. For this reason, one should be very careful while choosing the material card. Selection should be made in accordance with the simulation setup requirements to be established in the material card selection.

There are some points to be considered in determining the parameters. The parameters should be determined with the help of the relevant constitutive equations and then validated with a test setup to be made in the simulation environment, if possible.

Different material cards can be assigned to different parts used in numerical analysis. The definitions to be made vary according to the assumptions or outputs in the simulation setup to be established. In the sheet metal forming simulation setup, which is the subject of this thesis, rigid material was chosen for the tools. In many applications, if tool aging is not examined, tools are selected as rigid. Choosing a rigid material card also provides efficiency in terms of computational cost.

A selection must be made for the material card that is planned to be used for blank material. A series of test simulations were performed for this selection process. According to the simulation results, the material card was selected and used in the forming simulation.

Motivation of this part is to determine the most effective material card during the simulation of the sheet metal forming process. For this reason, two different material cards were examined, and material models was created using material test data of 316L stainless steel. Tensile test & hydraulic bulge test setups were created and the behavior of the material models in the numerical environment were compared with the test results.

The results were obtained from this was evaluated comparatively and the material model most suitable for the requirements of forming simulation was selected.

In the next stages, the material model was used in the numerical modeling of the sheet metal forming process.

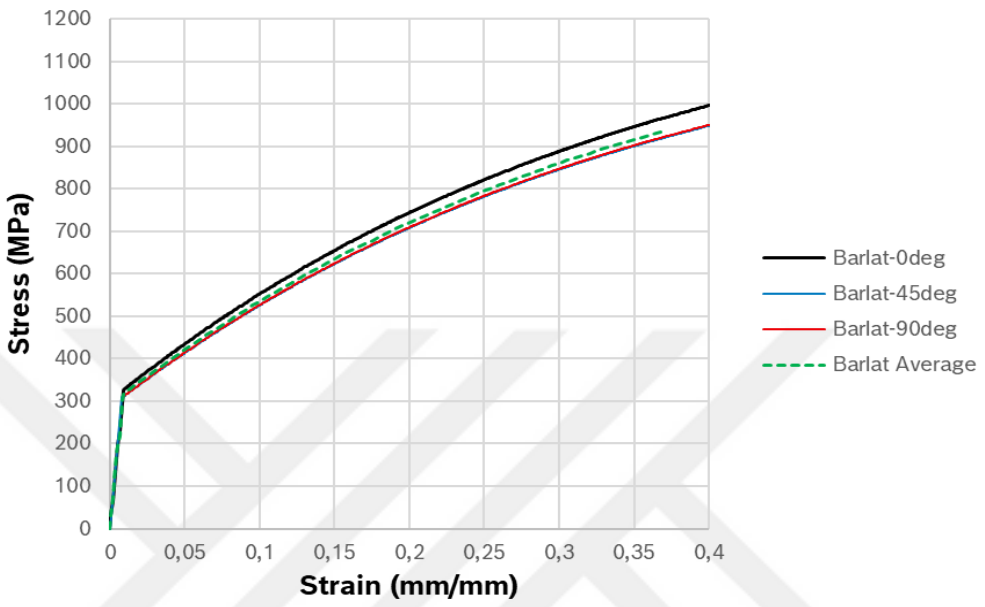


Figure 30. Numerical Tensile Test Results for 0/45/90 degree rolling directions and average with *MAT133_BARLAT_YLD2000 (Source: Gürler, Y. et.al, 2021)

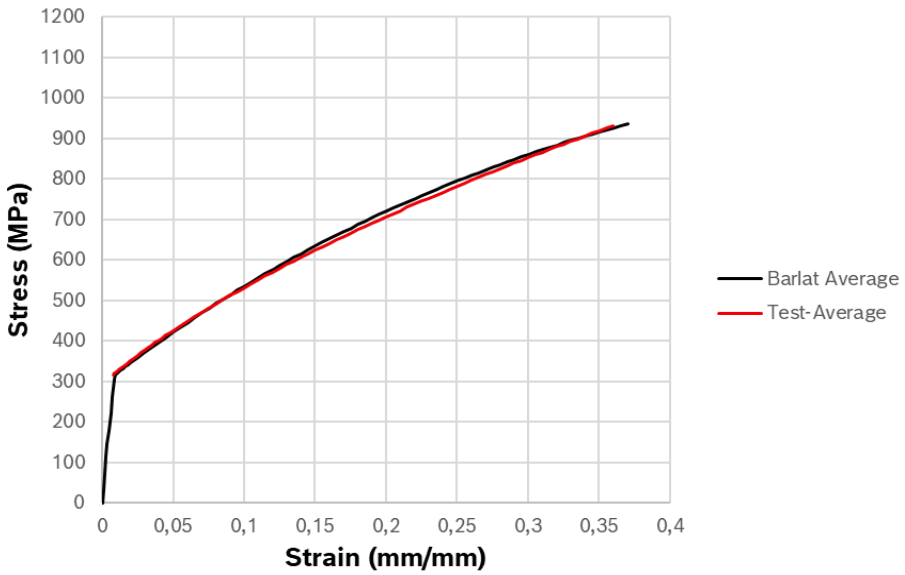


Figure 31. Comparison of numerical and experimental tensile test stress-strain results (Source:Gürler, Y. et.al, 2021)

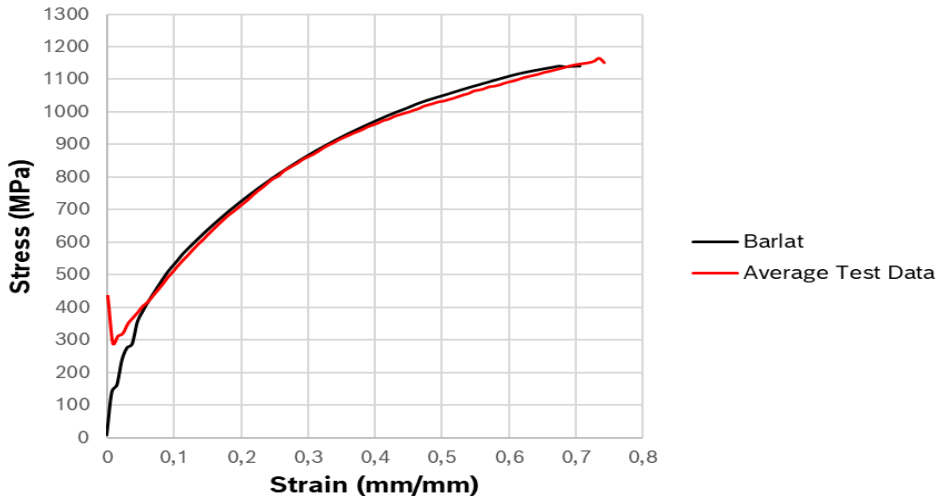


Figure 32. Comparison of numerical and experimental hydraulic bulge test stress-strain results [9] (Source:Gürler, Y. et.al, 2021)

### 4.4.1. Material Parameters

*MAT_RIGID material cards selected as tools material is as in the image below. The definitions of "RO: Mass density", "E: Elastic modulus" and "PR: Poisson's ratio" were made on these material cards. Also, the CMO option has been activated and selected as 1. EQ.+1 means; is to enable defining constraints in global directions. Represents "CON1: Global translational constraints". It is defined as "EQ.4: displacement constrained at x and y" for punch and die, and "EQ.7: displacement constrained at x, y, z" for blankholder. Represents "CON2: Global rotational constraints". It is defined as "EQ.7: x,y,z rotation constrained" for punch, die and blankholder.

*MAT_BARLAT_YLD2000 material card selected as blank material is as in the image below. The Barlat material model was chosen because of its easy adaptation to anisotropic behavior and strain rate sensitivity. Mechanical properties of the material are defined in section 1 of the picture below. These are "RO:Density", "E: Elastic Modulus", "PR: Poissons Ratio" respectively. In section 2, strain rate parameters are defined. These parameters were determined according to the dynamic test results using the Cowper-Symonds constitutive equation. C and P parameters are determined from the following equation.

$$\sigma_y^v(\varepsilon_p, \dot{\varepsilon}_p) = \sigma_y(\varepsilon_p)(1 + [\frac{\dot{\varepsilon}_p}{C}]^{\frac{1}{p}}) \tag{4.1}$$

In section 3, hardening type selection & hardening curve definitions are made. As the number -24, the yield stress as function of plastic strain curve with the Load Curve ID of 24 is defined. This curve is also known as the hardening curve. BCC material was defined as a flow potential exponent and “A=6” was determined.

In section 4, yield stresses, Lankford parameters, which are determined according to the static test results performed at 0-45-90 degrees, are entered. In section 5, the material Coordinate System is defined, and the direction in which the behavior of the material will change is set. Finally, in section 6, Components of vectors definitions are made.

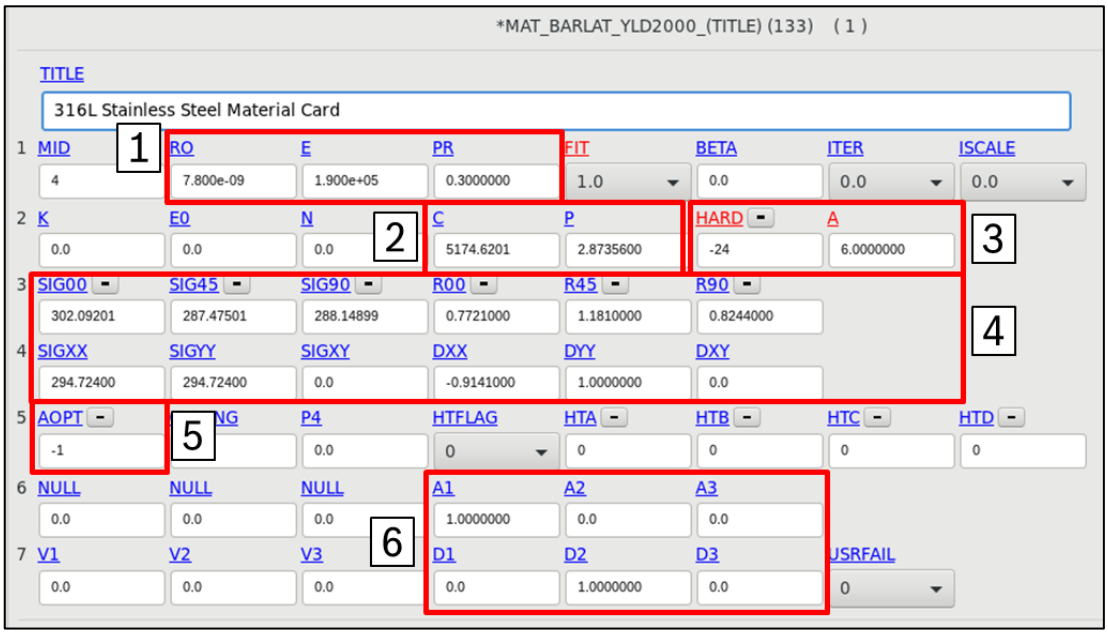


Figure 33. MAT_BARLAT_YLD2000 parameters in Ls-Dyna

# CHAPTER 5

# NUMERICAL MODELLING

Numerical modeling and simulation activities were carried out throughout the thesis. In this context, the definition of the problem whose numerical model was created is discussed in general terms. Numerical simulation setup and geometry simplification studies are mentioned. Information on the mesh structure and element formulations of the parts is also available. Afterwards, the material cards and parameters used during the numerical modeling activities are explained. In numerical modeling, contact definitions, boundary conditions (Tool speed, gas spring force etc.) and output definitions are also included. Finally, the details of implicit springback analysis are given.

## 5.1. Finite Element Analysis (FEA)

Finite element method (FEM) is a method used in the analysis of complex systems that cannot be solved with simple expressions. In the finite element method, systems with complex geometries are decomposed into elements of certain dimensions. As a result of this decomposition, many subsystems are formed in the system and are called finite elements. As a result of the creation of these small sub-elements, solutions can be obtained with the help of simple equations. Subsequently, this process is done for all the elements that are divided into parts. Ultimately, the subsystems that make up the whole of the system give an approximate result of the whole. The biggest motivation here is to divide the complex system into finite elements and converge the solution of the system with simple algebraic equations. The finite element method has been used effectively in our lives and in many sectors for many years. The use of the method accelerated with the widespread use of computers and took its place in the industry as an engineering method. Equations created with the help of computers can be easily solved. There are many different commercial software in the market that we can apply this method to. For example, Ansys, Ls Dyna, Abaqus, Hyperworks etc. The problem, which is the subject of this thesis, has been solved by using the finite element method and Ansys Ls-Dyna is used as a finite element analysis tool.[34]

### 5.1.1. LS-DYNA

Ls Dyna is a Finite Element Method based code used to solve static and dynamic structural analysis problems. Thanks to the explicit and implicit solver, it solves many structural analysis problems. As a solution method, there is explicit time integration at its core. It is frequently used in metal forming applications. Thanks to its adaptive remeshing and advanced element formulations, it gives very successful results for explicit form taking problems. Many different boundary conditions can be applied to the system in order to define the loads that occur during the process. Thanks to the wide material card options, it is possible to easily choose the material model suitable for the material to be used. Due to these factors, the finite element analysis program Ls-Dyna was chosen.[36]

### 5.1.2. General Steps of Finite Element Analysis of Sheet Metal Forming

There are some steps to be followed while performing finite element analysis. These will be briefly discussed in this section. Detailed steps are available in the following sections. First of all, a 3D CAD geometry is needed to perform finite element analysis. The 3D CAD model is checked with the help of a CAD tool and, if necessary, the model is cleaned. This cleaning is the cleaning of features that are thought to create unnecessary complexity and not affect the result. Then the mesh structure is created in 3D CAD files and the mesh files are imported into Ls-Dyna solver for assembly. Here, first of all, material definition is made for the geometries. Process boundary conditions are defined. The appropriate solution method is selected, and the simulation is run. After all the processes are completed, post-processing is done in order to make the result files meaningful and to make comparisons. During the post-process, necessary adjustments are made for the desired outputs and reported if necessary.

## 5.2. Numerical Modelling

Numerical study was carried out with LS-DYNA explicit finite element method software. Both SpaceClaim and Hypermesh were used for drawing, simplification (shown in figure 34) and meshing the model. Ls-PrePost was used for creating parts of numerical model and monitored the results. The solution time was reduced by modeling the tools

and blanks as shell elements. Springback effect was adapted in Ls-Dyna environment after forming simulation. The determined parameters from mechanical tests were used in the *MAT_YLD2000_BARLAT (MAT_133) material model[3], which allows to define material properties in anisotropic materials with strain rate sensitivity.

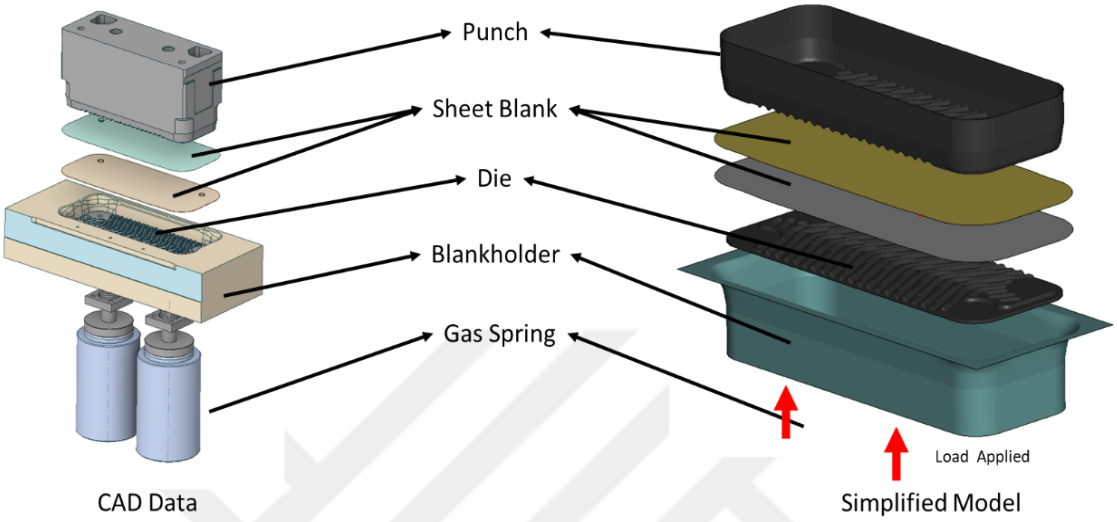


Figure 34. CAD Data vs. Simplified Model

## 5.3. Mesh

Blank is meshed with 1 mm element size. Quad element used for the mesh operations. The mesh was divided into sections in order to have high quality on the blank part. In the tools, various sizes are set in the range of 0.5mm-2mm. Since the tool is rigid, the mesh size does not have a load on the explicit simulation. For this reason, mesh is used in the dimensions that will give the most suitable shape of the tools. In figure 35 below, the images of the meshed geometries are available.

The quality of the mesh created on the blank was examined, it was observed that the Aspect Ratio had elements less than 1.77 in figure 36. On the other hand, the min time-step, which is important for explicit analysis, was also examined and found to be 1.226E-7. This mesh requires a computational power that will force the simulation even on you. When the other parameters related to mesh quality were examined, it was determined that the Skewness value was max 0.35 and the normalized Jacobian value was min 0.8.

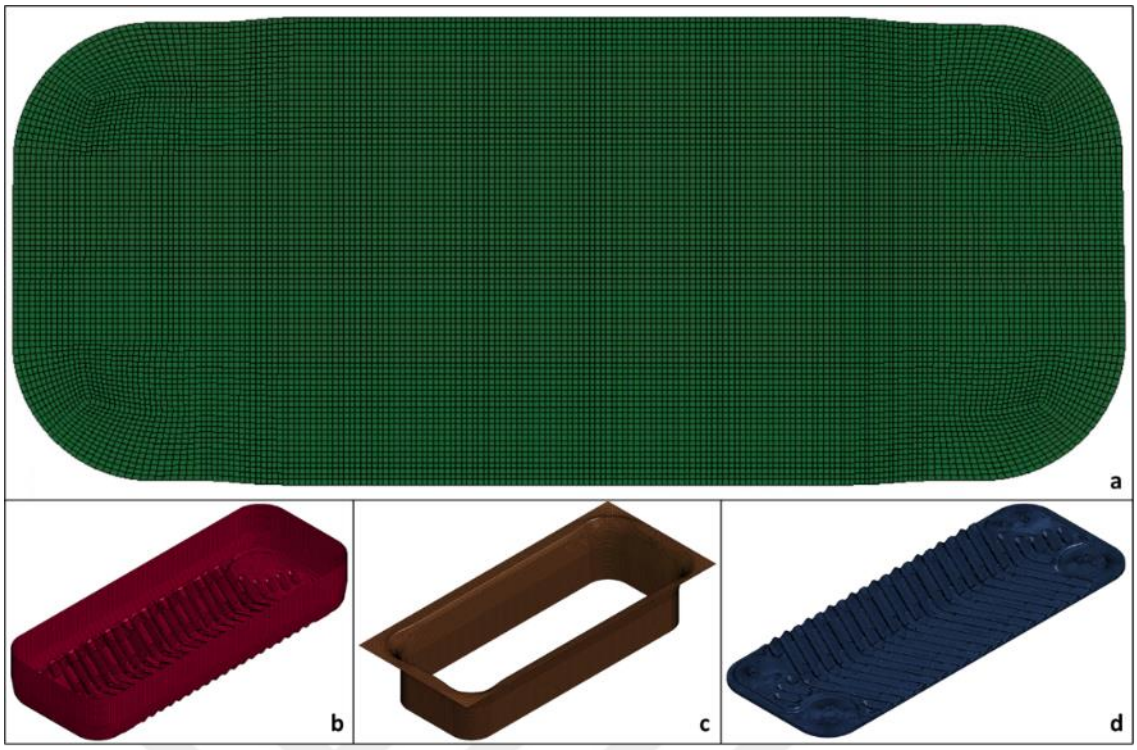


Figure 35. Blank (a), Punch (b), Blankholder (c), Die (d)

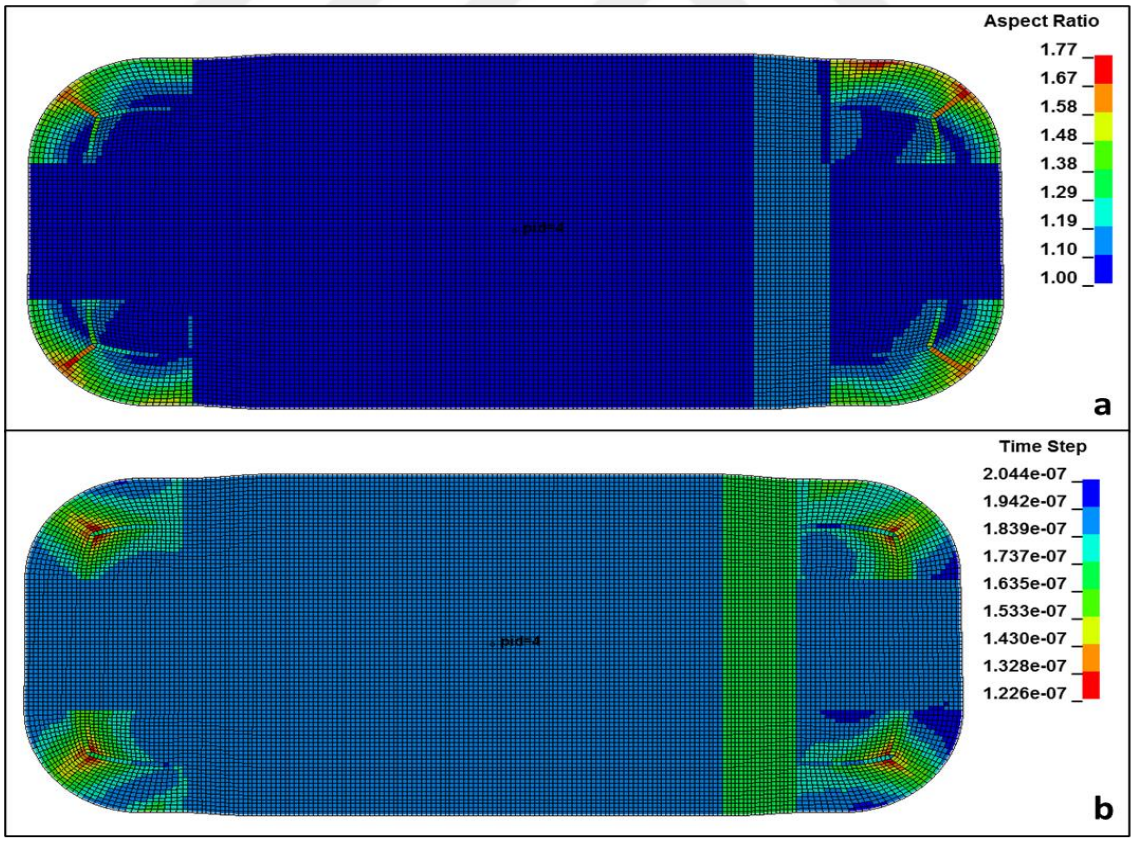


Figure 36. Aspect ratio and time step size of the blank

### 5.3.1. Mesh Sensitivity

Mesh sensitivity analysis were performed with 0.5 mm, 0.75mm, 1mm, 1.25mm, 1.5mm blank sizes. Based on the analysis results, 1mm blank size has been selected and the comparisons of the outputs are as follows. First, the reason why the largest mesh size of 1.5 mm was chosen is because the geometry to form is complex, resulting in errors. As can be seen from the results, singular stress values were observed in the numerical model with a mesh size of 1.5 mm. On the other hand, the min thickness value decreased until the 0.75 mm mesh size threshold and then started to increase. For 0.5 mm, it was dissolved for close to 50 hours and unfortunately the analysis could not be terminated. Even when the values taken from the point of the analysis are taken as a basis, differences in stress and thickness values are observed. Based on the stress and thickness and solution time values, it makes sense to proceed with 1 mm based on the sensitivity analysis.

Table 9. Solution time according to mesh sizes

| Mesh Size (mm) | Solution Time |
|---|---|
| 1,50 | 4 hours 23 minutes |
| 1,25 | 6 hours 16 minutes |
| 1,00 | 8 hours 6 minutes |
| 0,75 | 17 hours 17 minutes |
| 0,50 | more than 50 hours |

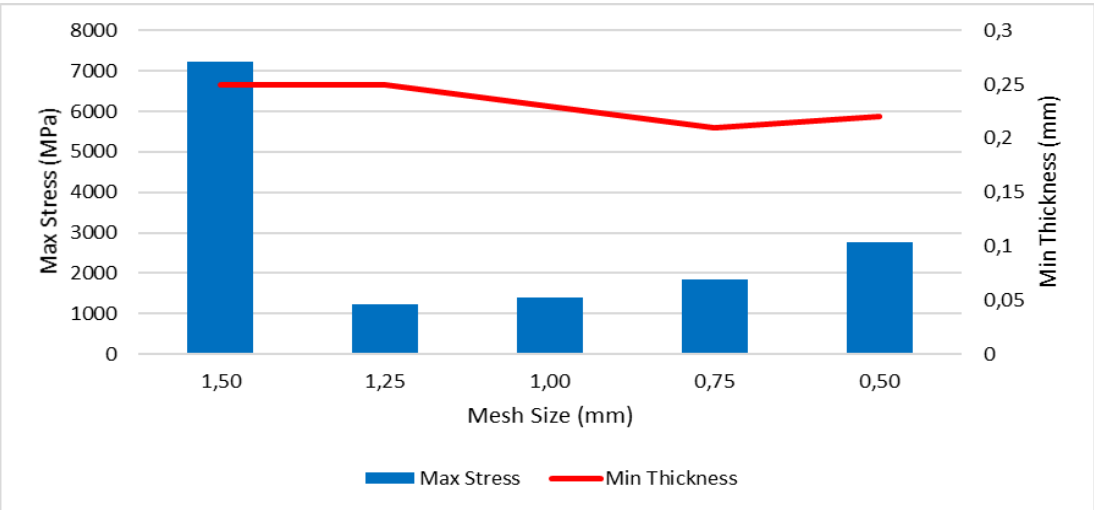


Figure 37. Mesh sensitivity outputs regarding to different mesh sizes

## 5.4. Element Formulation

Shell element formulation is an element type that is frequently used in sheet metal forming simulations. In this thesis, tools and blank are modeled with shell element formulation.

Shell parts used in the tools are modeled as "EQ.16 Fully Integrated Shell Element" as element formulation. In addition, 3 numbers of integration points were used in the numerical model. A value close to the blank thickness was chosen as the thickness, but the tool was modeled as the top surface, not the mid-surface. For this reason, thickness does not matter. It is integrated into the model by selecting EQ.1 under NLOC that the reference surface is the top surface.

Shell parts used in Blank are also modeled as "EQ.16 Fully Integrated Shell Element" as element formulation. However, 5 numbers of integration points are used here. The value of 0.3mm, which is the blank thickness, was entered as the thickness. Blank is modeled as a mid-surface. For this reason, NLOC EQ.0 was chosen, where the reference surface is the mid-surface. [37]

## 5.5. Contact

*CONTACT_AUTOMATIC_SURFACE_TO_SURFACE was used between blank and blankholder. *CONTACT_FORMING_SURFACE_TO_SURFACE was used between blank and punch, blank and die. Master and slave type selected as part number. Due to the lubricant usage in the forming operation, friction coefficient was assumed the 0.1. Penalty formulation (EQ.0) is selected as soft option. Shell element thickness setting was selected as SHLTHK:2, including rigid bodies.

## 5.6. Tool Motion

*BOUNDARY_PRESCRIBED_MOTION_RIGID was used to determine punch velocity. Movement of punch was described with displacement curve along z direction. DOF was selected EQ.3 for z-direction. VAD was selected EQ.2 for displacement definition. There is no scale factor used in the curve.

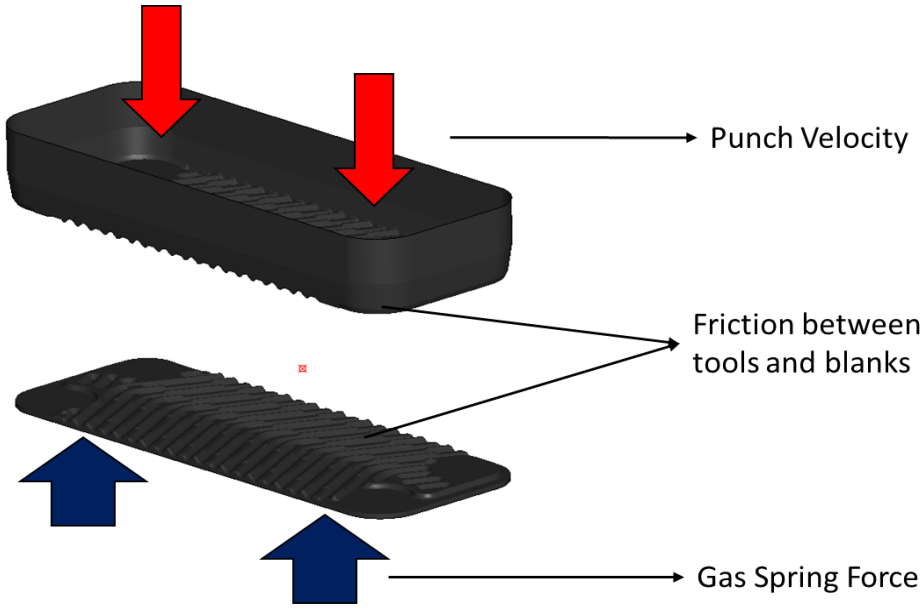


Figure 38. Applied load and velocity for tools

## 5.7. Gas Spring Force

*LOAD_SEGMENT_SET was used to determine load from gas springs. Load of gas-springs was described with MPa-time curve along z direction (figure 40). Applied load selected as segment set shown in below (figure 39). There is no scale factor used in the curve.

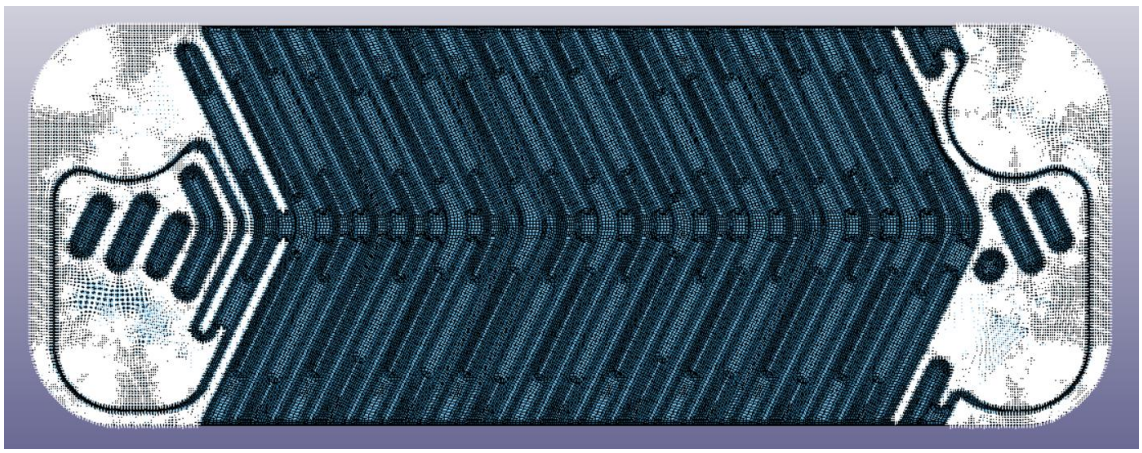

Figure 39.Segment set for gas spring loads

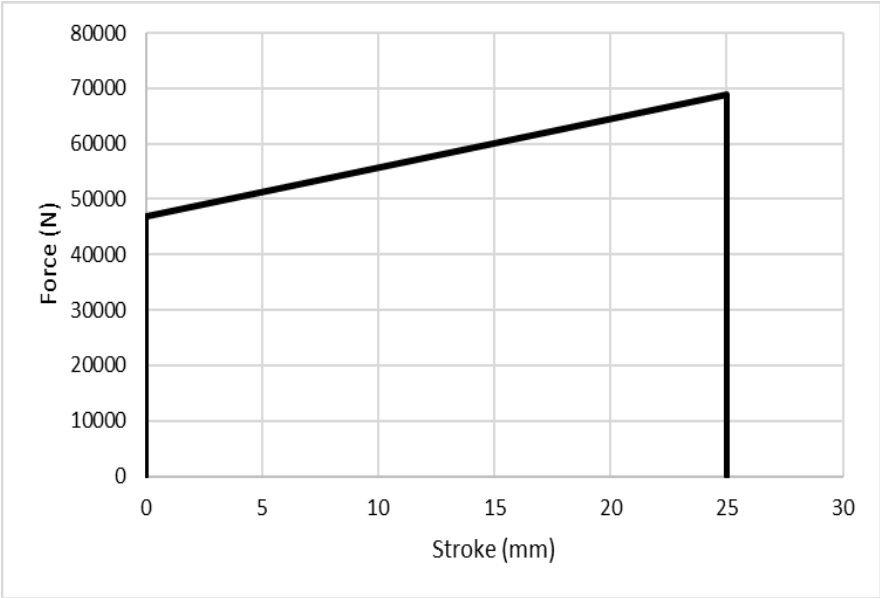


Figure 40. Characteristic Load Curve for Gas Springs

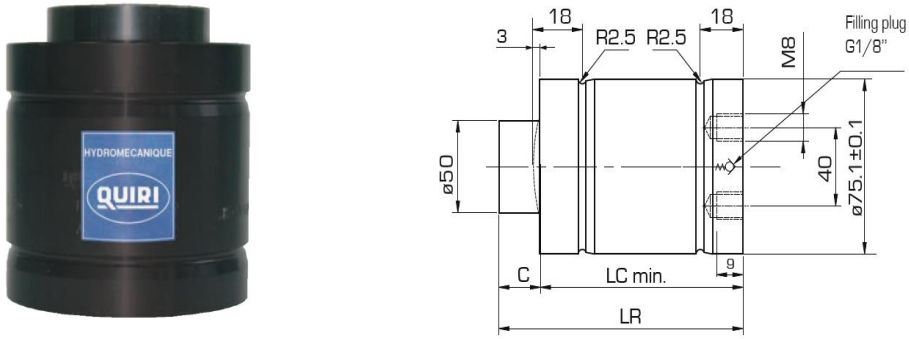


Figure 41. Gas Spring and Technical Details

(Source: Quiri, 2023)

## 5.8. Outputs & Solver Options

In numerical analysis outputs, GLSTS, MATSUM, NODFOR, NODOUT, RCFORC settings are activated respectively in ASCII settings to be used in post process. In addition, DATABASE_BINARY_D3PLOT and EXTENT_BINARY cards are also used. HPC Cluster was used as solver. The simulation was solved by dividing the 16 cores into 8 along with 128 cores in the MPP solver.

## 5.9. Springback

*INTERFACE_SPRINGBACK card allows LS-DYNA to conveniently export geometry with residual stresses and strains. Picture below was determined for export as a dynain file the geometry. Parts which needed to export defined as part set in PSID.

After the dynain file created in solution file, the dynain file comes in Ls-Dyna with residual stress and residual strain inputs. Then create a case using springback via eZsetup. The dynain file and the material card are automatically given as input together. Then eZsetup creates an input k file for the springback operation. After running in the k-file solver, the final result is obtained.

# CHAPTER 6

# RESULT AND DISCUSSIONS

The purpose of this chapter is to give information about the results of the experimental and numerical activities carried out throughout the thesis. In this context, the results of the tests carried out and supported by the outsource, these are the uniaxial tensile test, hydraulic bulge test, split Hopkinson tension test, respectively. On the other hand, the outputs obtained from the numerical modeling activities are also included in this section. Validation of the numerical and experimental model is also the subject of this chapter.

## 6.1. Sheet Metal Forming Results

The 3D scanning method was used to compare the sample produced as a result of the sheet metal forming operation with the numerical analysis outputs. Thanks to this method, the sample taken from the production was scanned by the 3D scanning machine, the 3D model was created, and the thickness distribution analysis was performed. The scan results obtained are shown below.

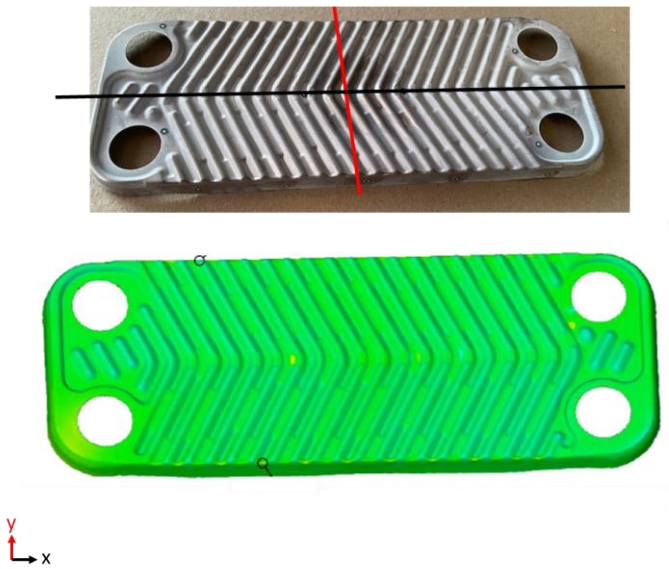


Figure 42. Scanning results of PHE plate

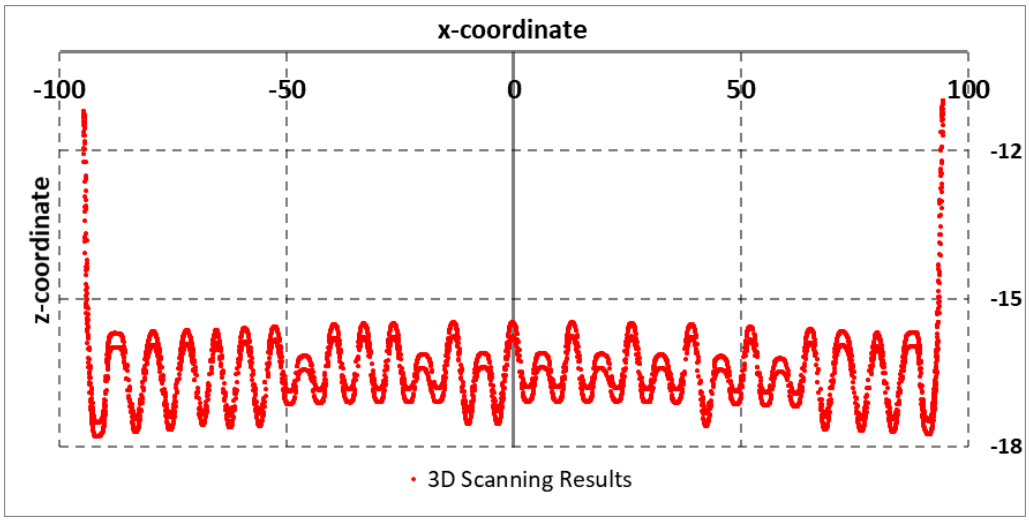


Figure 43. Cross section of the PHE plate along the y-axis from middle of the plate

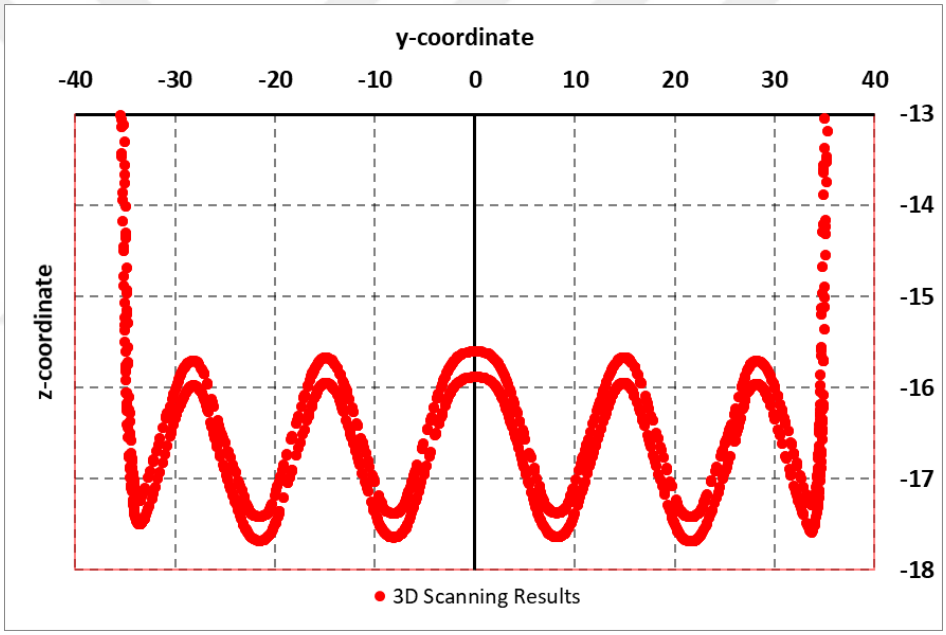


Figure 44. Cross section of the PHE plate along the x-axis from middle of the plate

Residual stresses were measured on 316L stainless steel PHE plate with XRD method, measurements were caried out with 2-circle portable deflactometer and 1 mm spot was used. According to EN 15305:2008 standard Mn- Kα radiation on (3 1 1) planes of austenitic stainless steel were used and all test carried out Simultura Material Technologies labaratories [35] The pricipal stress values obtained from the plates using the XRD method, Von-Misses stresses were calculated using the following principal plane stress equation. The calculated Von-Misses stress (equation 6.1) values give the residual stress values remaining on the plate.

Table 10. XRD Measurement Result

| | **Measurement Point1** | **Measurement Point2** | **Measurement Point3** |
|---|---|---|---|
| **$\sigma_1$** | 66,6 MPa | 16,3 MPa | -44,9 MPa |
| **$\sigma_2$** | 8,9 MPa | -92,5 MPa | -110,2 MPa |
| **Residual Stress** | **62,6 MPa** | **101,6 MPa** | **96,0 MPa** |
| **Tolerances (+/-)** | 18,3 MPa | 21,4 MPa | 80,5 MPa |
| **Max Residual Stress** | 80,9 MPa | 123,0 MPa | 176,5 MPa |
| **Min Residual Stress** | 44,3 MPa | 80,2 MPa | 15,5 MPa |

$$\sigma_v = \sqrt{\sigma_1^2 - \sigma_1\sigma_2 + \sigma_2^2} \tag{6.1}$$

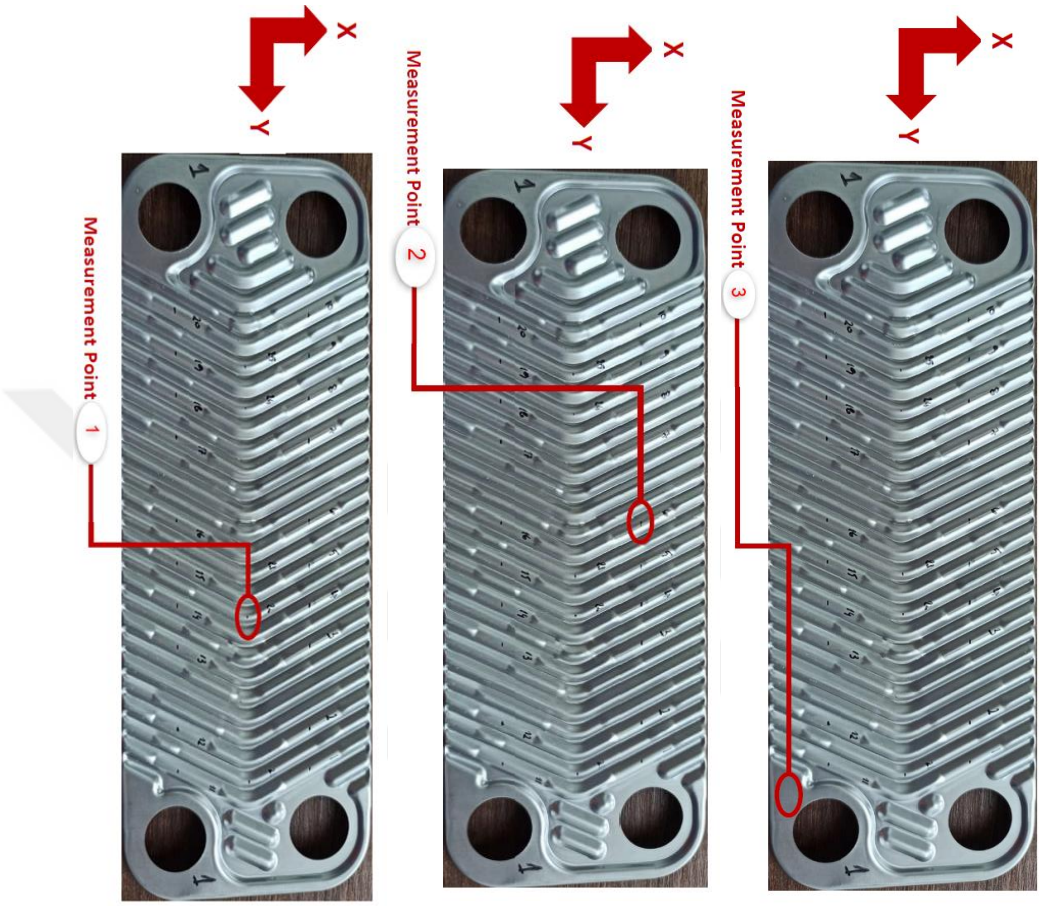


Figure 45. XRD Measurment Points

The table below shows the values calculated using the pricipal plane stress equation and the principal stress values given by the measurement center. In addition, the tolerance values given by the measurement center are also included in the table. In the light of this information, the maximum and minimum value of the calculated residual stress value was determined.

## 6.2. FEA Results

FEA results are analyzed in this section. First, the maximum stress values were examined in the process stage, and the stress regions are shown in the figures below. In the two analyzes performed under the same boundary conditions, the only difference is

the material type. According to the change of material type, 1408 MPA maximum effective stress was observed in the analysis for 316L stainless steel. In the analysis made for 304 stainless steel, a maximum effective stress of 1240 MPA was observed.

Table 11. Maximum Effective Stress Values of PHE Plates

| Material | Maximum Effective Stress (MPa) |
|---|---|
| 316L | 1408 |
| 304 | 1240 |

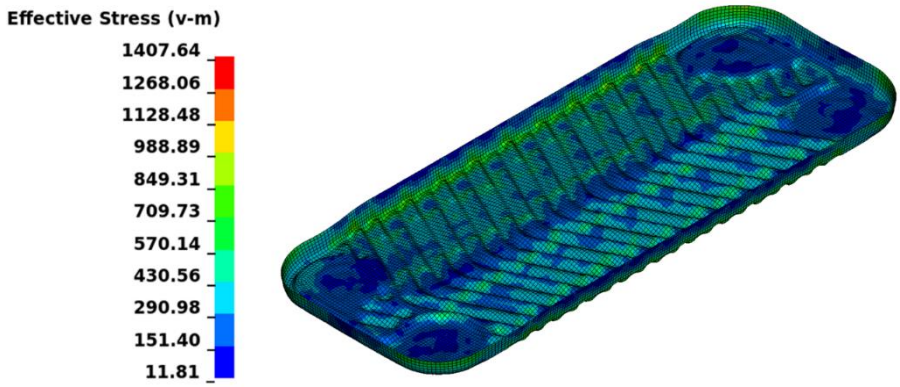


Figure 46. Effective stress of 316L stainless steel PHE plate

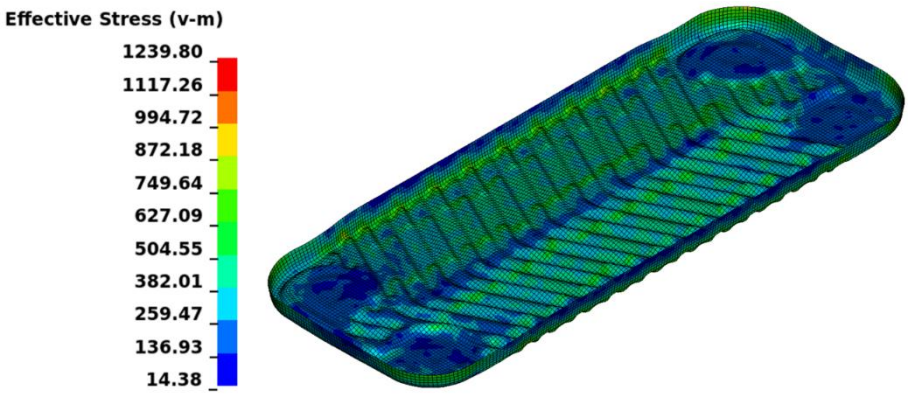


Figure 47. Effective stress of 304 stainless steel PHE plate

Residual Stresses are one of the outputs of that study. After the springback stage occur, residual stresses can be seen below. According to the material type, 1124 MPA residual stress was observed in the analysis for 316L stainless steel. 1138 MPA residual stress was observed in the analysis for 304 stainless steel.

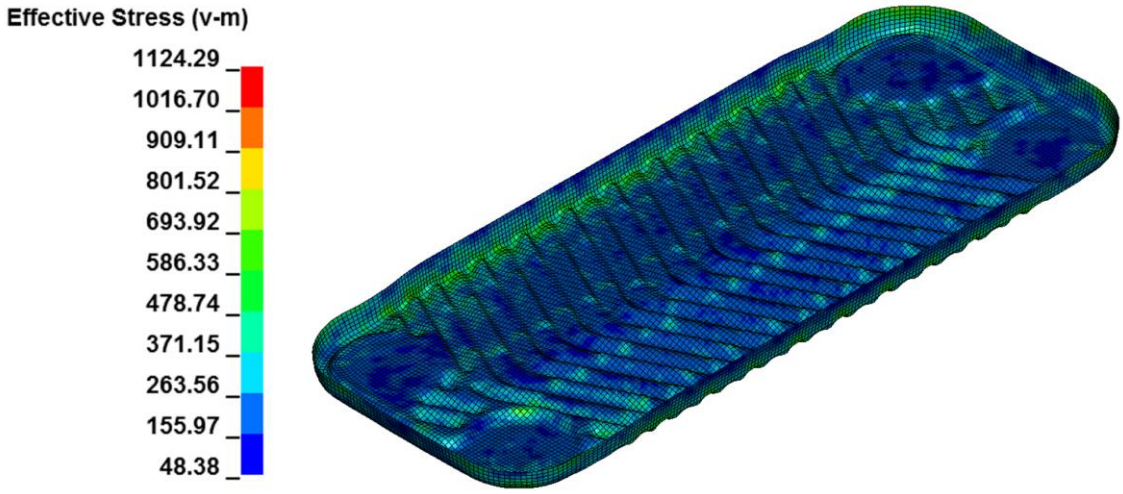


Figure 48. Residual stress of 316L stainless steel PHE plate

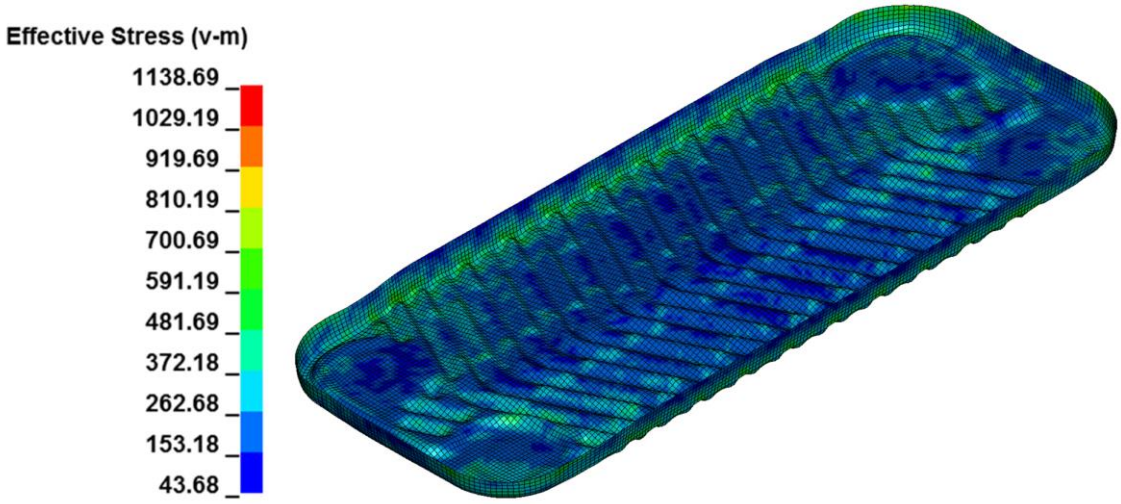


Figure 49.Residual stress of 304 stainless steel PHE plate

Table 12. Residual stress of stainless steel PHE plates

| Material | Residual Stress(MPa) |
|---|---|
| 316L | 1124 |
| 304 | 1138 |

As another FEA analysis output, the effective plastic strain results were compared. In the analysis made for 316L stainless steel, 0.28 maximum plastic strain was observed. In the analysis made for 304 stainless steel, 0.26 maximum plastic strain was observed.

Table 13. Maximum effective plastic strain values of PHE plates

| Material | Maximum Plastic Strain (m/m) |
|---|---|
| 316L | 0,28 |
| 304 | 0,26 |

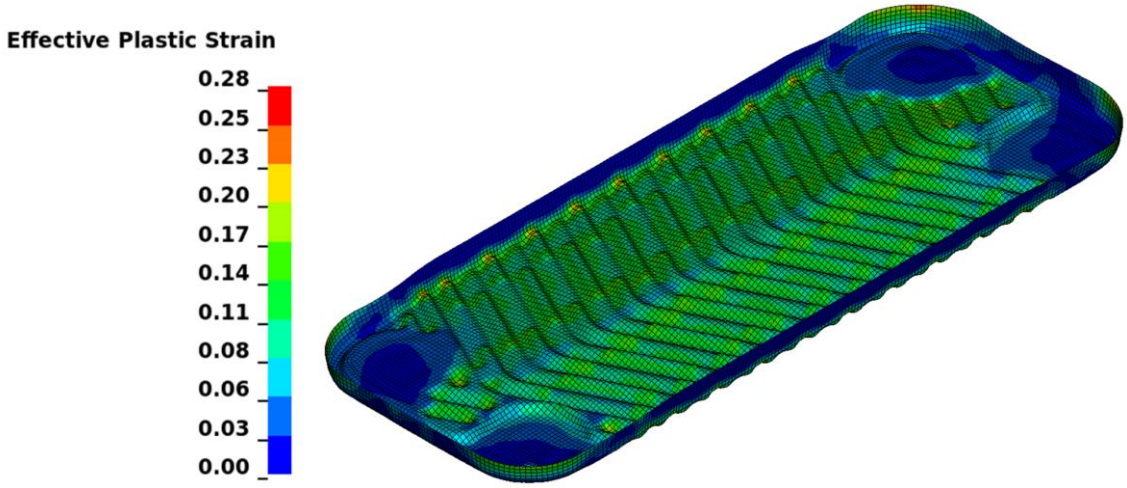


Figure 50. Effective plastic strain of 316L stainless steel PHE plate

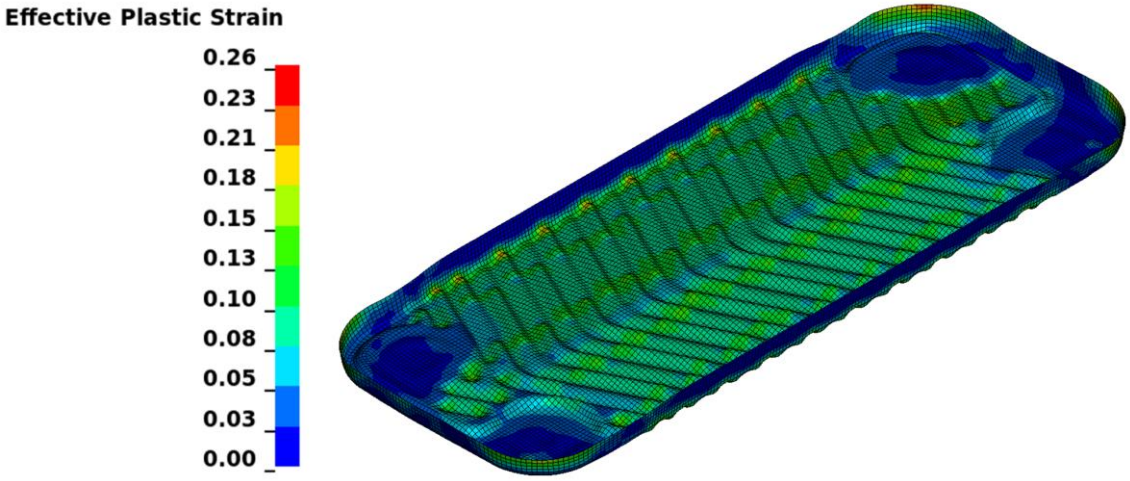


Figure 51. Effective plastic strain of 304 stainless steel PHE plate

Shell thickness values were also examined as output, and the thickness distribution for 316L and 304 material is as follows. When 316L stainless steel was examined, the maximum thickness was observed in the corners and bends and was determined as 0.35mm. Likewise, when looking at the minimum thickness values, it was

observed that it was in the pit areas, and it was determined to be 0.23 mm. When 304 stainless steel was examined, the maximum thickness was obser0ved in corners and bends as in 316L, but it was determined as 0.34mm. Likewise, when looking at the minimum thickness values, it was observed that it was in the pit areas, but it was found to be 0.25 mm. As it can be understood from here, 304 stainless steel showed less ductile behavior than 316L stainless steel.

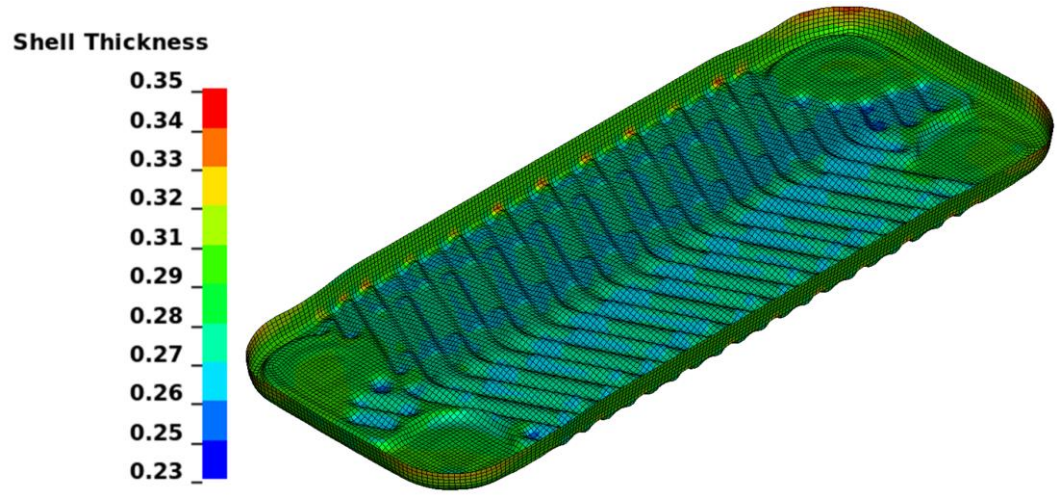


Figure 52. Shell thickness distribution of 316L stainless steel PHE plate

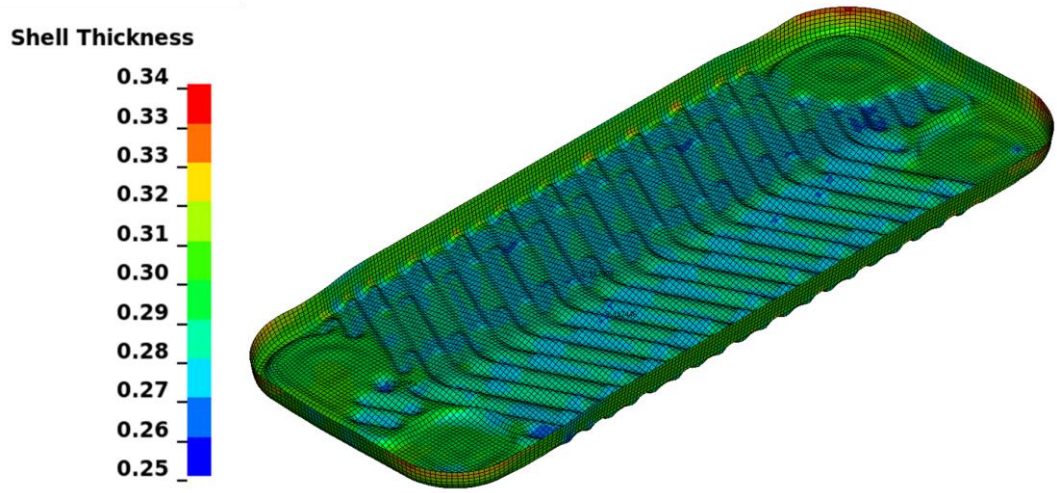


Figure 53. Shell thickness distribution of 304 stainless steel PHE plate

Another parameter that should be examined after the shell thickness value is the thickness reduction value. Here, there are three region which named as Valley, Hill, and Hole. The regions are shown in the figure below. 316L and 304 stainless steels were compared for these 3 regions. When the valley region is examined, a thickness decreases

of 10.87% was observed for 316L stainless steel material, while a 9.45% thickness reduction was observed for 304 stainless steel material. When the Hill region is examined, 14.05% thickness reduction is observed for 316L stainless steel material, while 12.2% thickness reduction is observed for 304 stainless steel material. When the hole area is examined, 17.19% thickness reduction is observed for 316L stainless steel material, while 13.5% thickness reduction is observed for 304 stainless steel material.

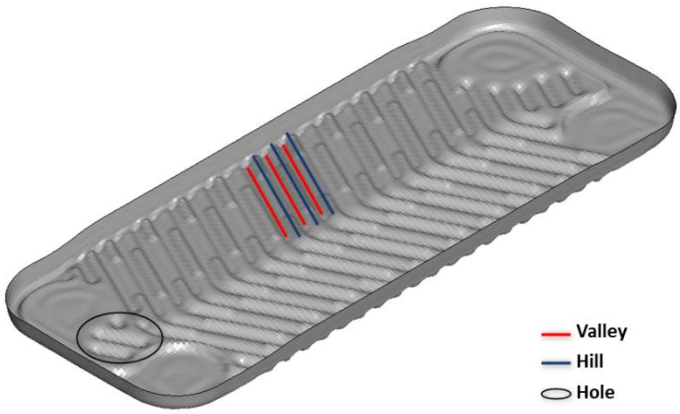


Figure 54. Critical thickness reduction areas of PHE plate

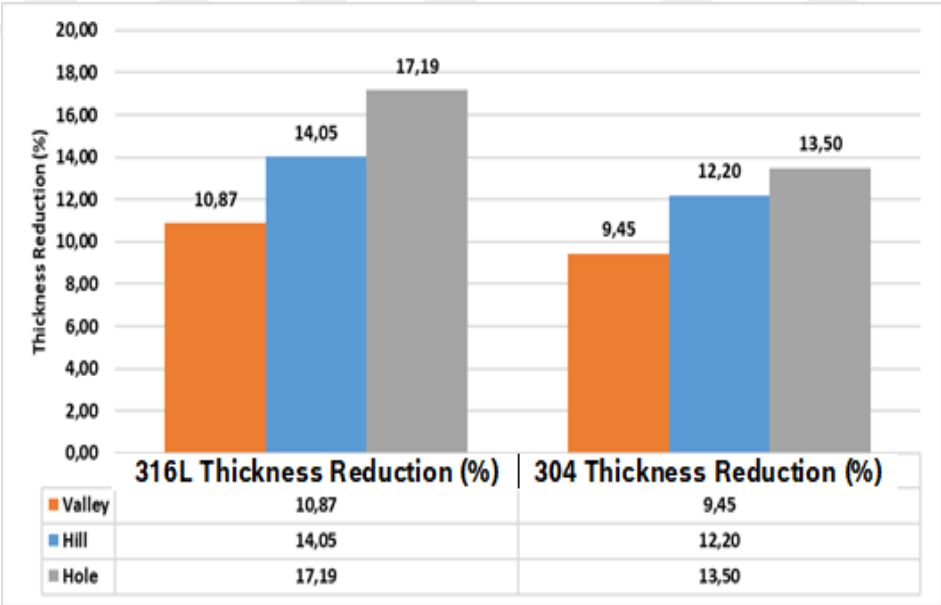


Figure 55. Comparison of the thickness reduction ratios of 316l & 304 stainless steel

Cross-section along the y-axis comparison was also made for two different materials. It has been observed that there are differences in the peaks between the materials and are available in the figures below.

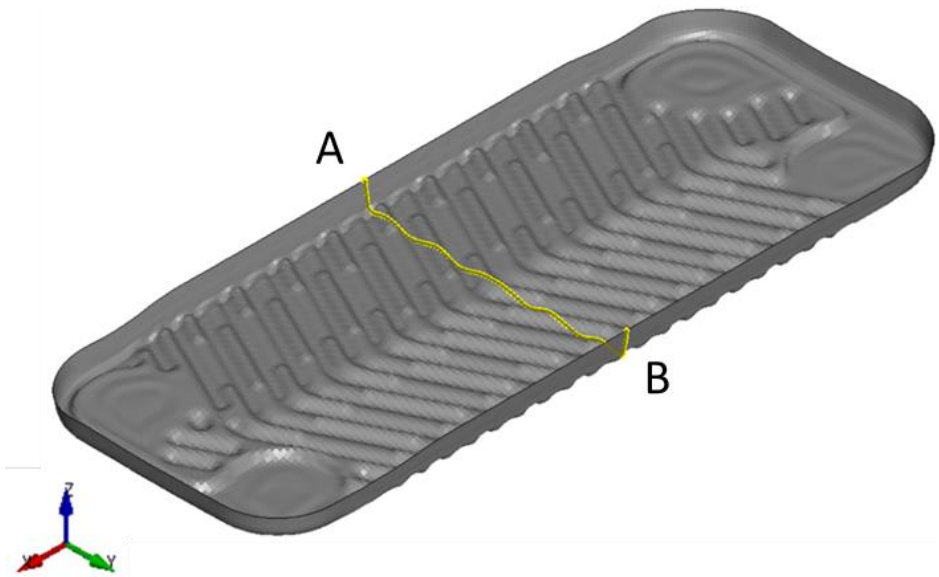


Figure 56. Plate cross-section along y-axis

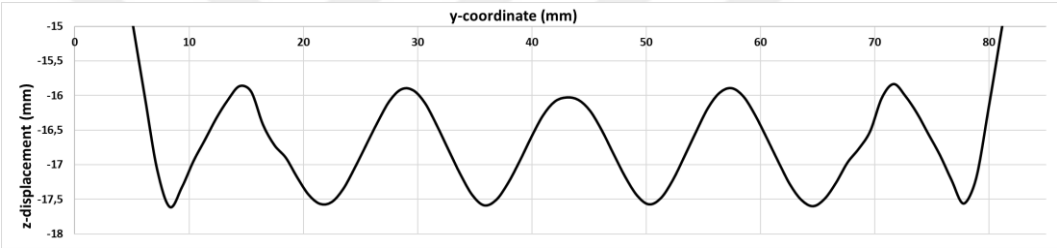


Figure 57. 316L stainless steel z-displacement along y-axis from A to B

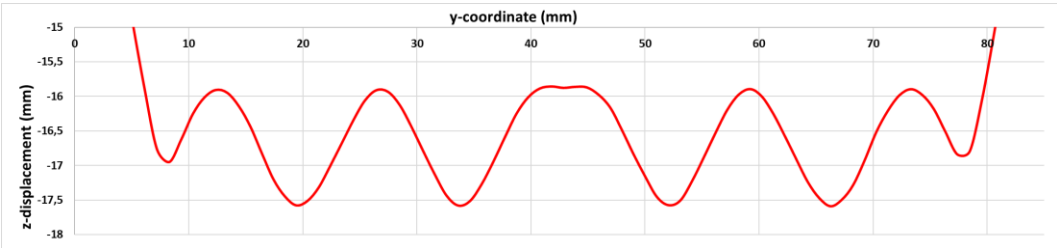


Figure 58. 304 stainless steel z-displacement along y-axis from A to B

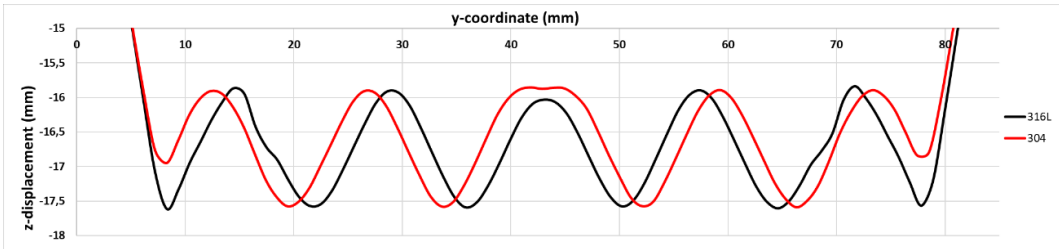


Figure 59. Comparison of 316L&304 z-displacement along y-axis from A to B

Cross-section along the x-axis comparison was also made for two different materials. It has been observed that there are differences in the peaks between the materials and they are available in the figures below.

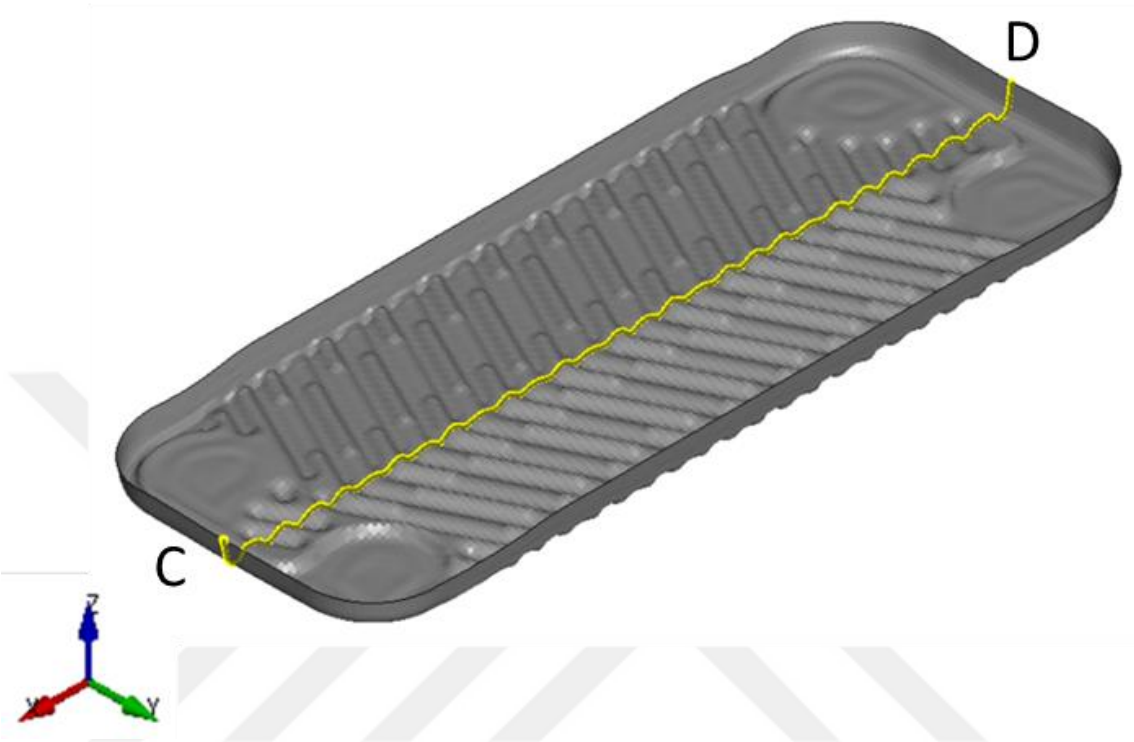


Figure 60. Plate cross-section along x-axis

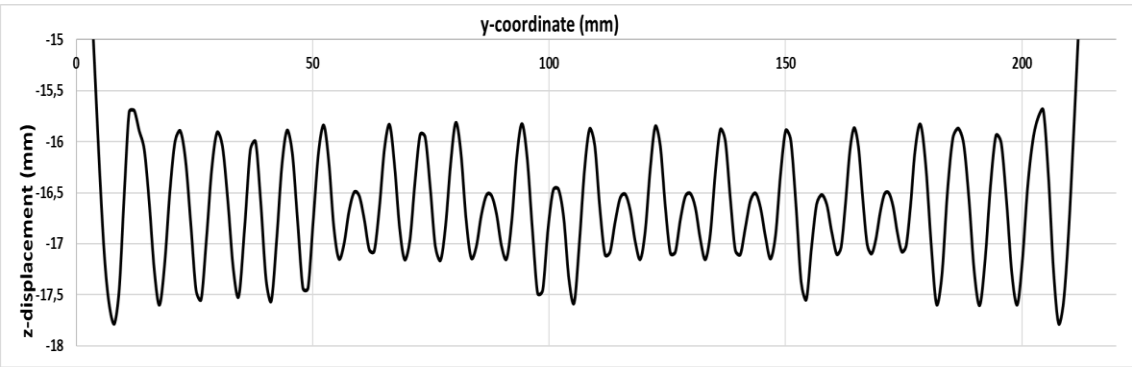


Figure 61. 316L stainless steel z-displacement along x-axis from C to D

The results obtained on the final shapes along the x and y axis of 316L and 304 stainless steel were compared. The compared results show that although the boundary conditions are the same, the form that the 316 L stainless steel takes at the peak and trough points is not observed in the 304 stainless steel. Here, two different materials have caused deltas between each other. These differences also show that 316L stainless steel exhibits

a more ductile behavior than 304 stainless steel material. On the other hand, 316L stainless steel has taken a shape more similar to the final geometry and it has been observed that different process parameters are needed for 304 stainless steel to take the form of the same final geometry.

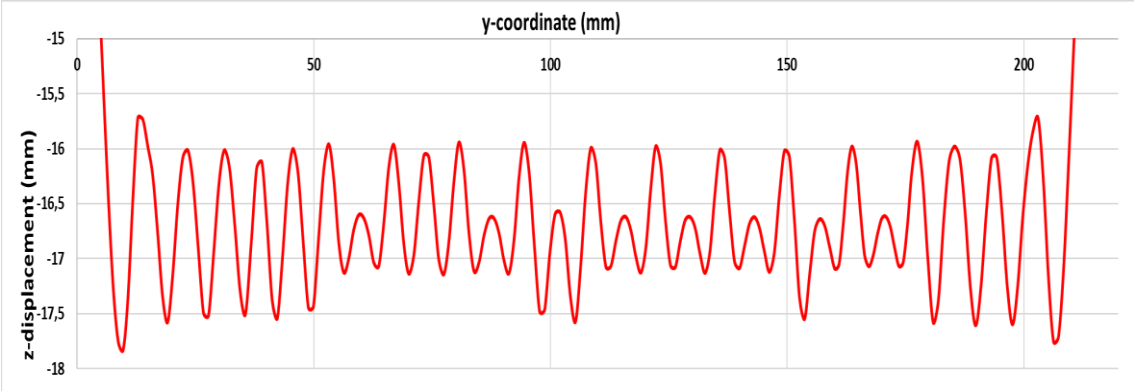


Figure 62. 304 stainless steel z-displacement along x-axis from C to D

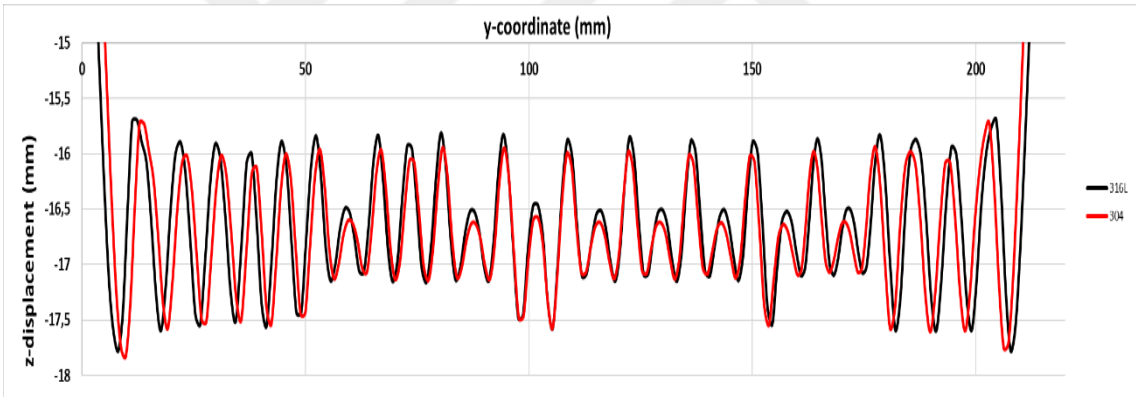


Figure 63. Comparison of 316L & 304 stainless steel z-displacement along x-axis from C to D

## 6.3. Validation of Numerical Approach

In order to prove the accuracy of the numerical model, the forming performances in the x and y axes were compared. The sample taken from the production line was scanned with 3D scanning method. The geometry obtained as a result of this process and the comparison of the geometries formed as a result of the FEA analysis are as in the graphs below. As seen in the results, the production sample and the shape formed as a result of FEA overlap. As a result of the FEA analysis, the desired shape was given. Outputs are consistent with production results.

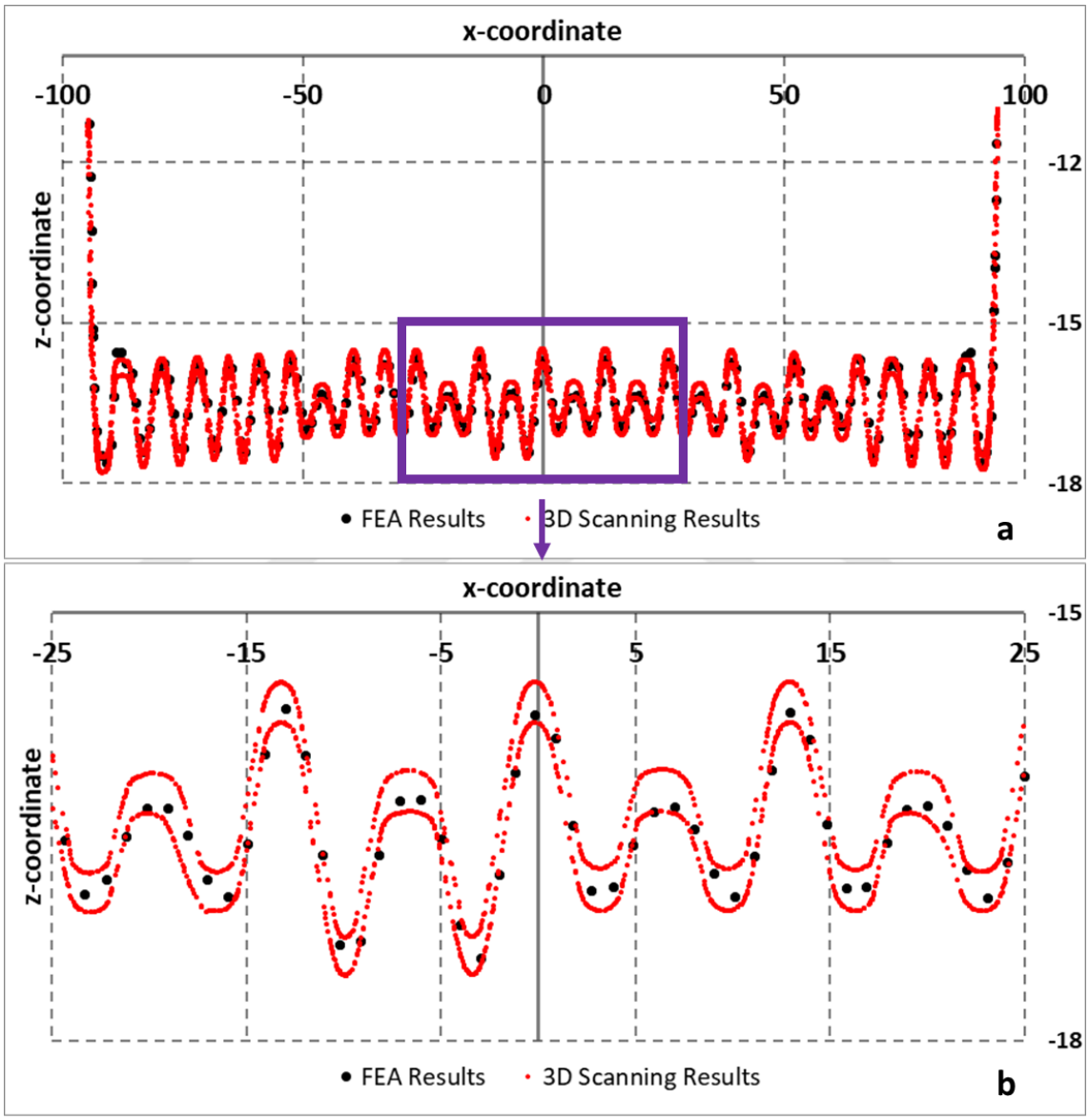


Figure 64. Cross section along the x axis comparison between 3D scanned part and FEA result for 316L, a- General View, b- Detailed View

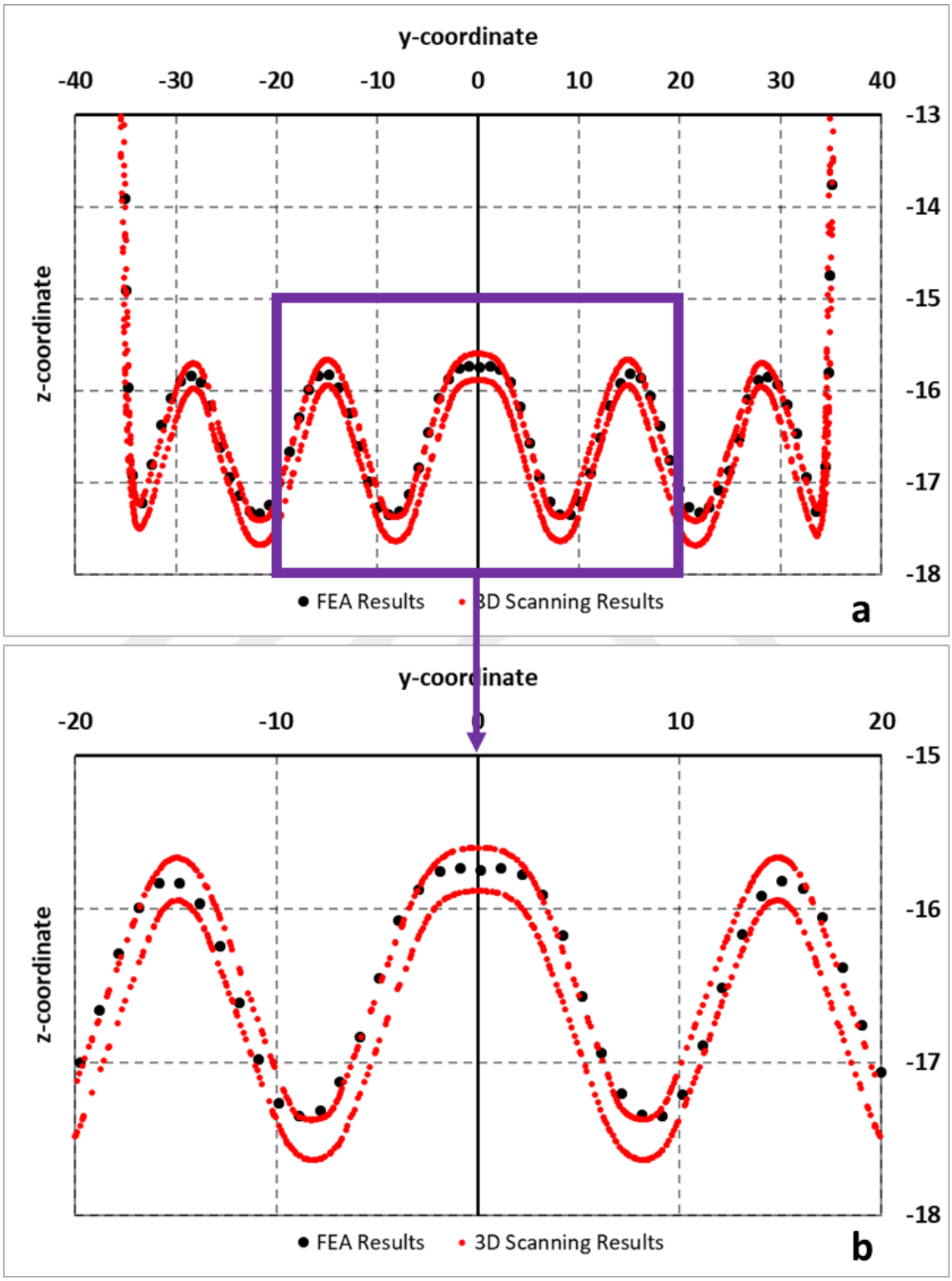


Figure 65. Cross section along the y axis comparison between 3D scanned part and FEA result for 316L, a- General View, b- Detailed View

The FEA results were read over 4 elements for residual stress to compare with XRD measured points and the average values were calculated. The reason for reading on 4 elements is that the measurement was made from a 2mmx2mm area, so 4 elements with an element size of 1mmx1mm will give us an approximate result. In the table below, the FEA results are calculated as element based and average.

Table 14. FEA Results of Residual Stresses for XRD Measurement Points

| | **Measurement Point1** | **Measurement Point2** | **Measurement Point3** |
|---|---|---|---|
| Element1 | 73,2 MPa | 103,0 MPa | 152,6 MPa |
| Element2 | 31,7 MPa | 106,7 MPa | 144,8 MPa |
| Element3 | 35,6 MPa | 97,4 MPa | 167,7 MPa |
| Element4 | 77,6 MPa | 72,4 MPa | 161,2 MPa |
| **Average** | **54,5** MPa | **94,9** MPa | **156,6** MPa |

The results of the regions calculated by XRD method and compared with FEA results are given in the table below. According to the information obtained, FEA results are within the tolerance band of the measurement results. The outputs of the simulation model coincide with the measurement results.

Table 15. Comparison between XRD Measurement Results and FEA Results

| | **XRD Measurement Result** | **FEA Result** |
|---|---|---|
| **Measurement Point1** | between 44,3 MPa-80,9 MPa | 54,5 MPa |
| **Measurement Point2** | between 80,2 MPa-123 MPa | 94,9 MPa |
| **Measurement Point3** | between 15,5 MPa-176,5 MPa | 156,6 MPa |

## 6.4 Forming Limit Diagram

After the forming limit diagram (FLD) obtained from the Nakajima tests was imported into the Ls-Dyna interface, cracks, risky and safe areas on the formed material were determined as the figure above was shown. Referring to the major and minor strain values, the graph showing in which region all the elements found on the formed geometry are located is given below.

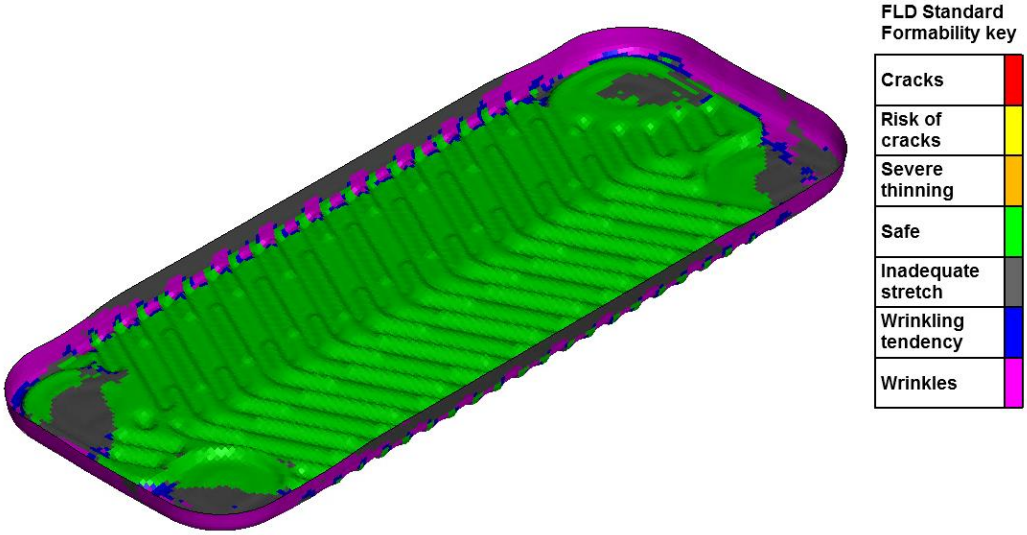


Figure 66. Numerical results of the plate according to FLD curve

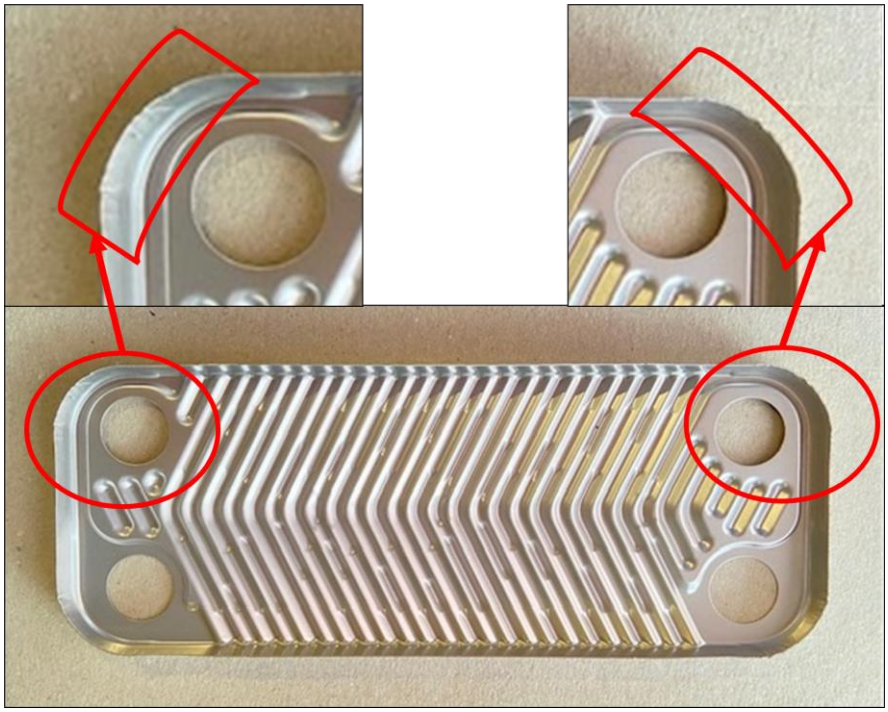

Figure 67. Wrinkles area on the plate

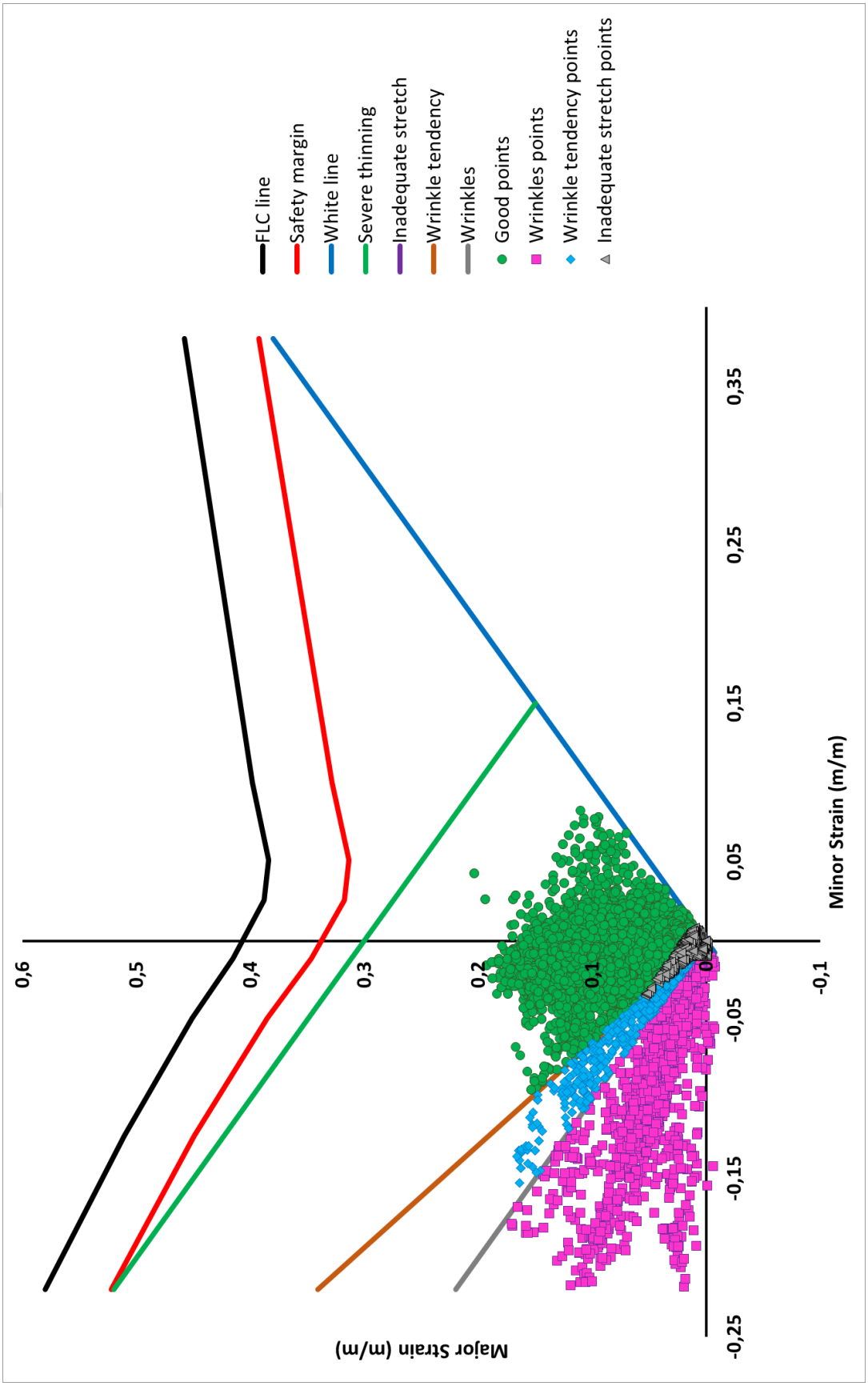


Figure 68. Element-base major minor strain of the plate for 316 L Stainless Steel in FLD

Table 16. Results from FLD

| Category | (%) |
|---|---|
| Safe | 73,7 |
| Wrinkles | 11,5 |
| Wrinkles Tendency | 2,9 |
| Inadequate Strectch | 11,9 |

According to the results there is no crack or risk of crack was not observed in the numerical model and the experimental model. It appeared as a pattern safe area which is %73.7 of the plate in the middle area, where the actual heat transfer takes place, and inadequate stretch areas which is %11.9 of the plate were formed towards the edges. The edges are observed as wrinkles which is %11.5 of the plate along the circumference of the plate. Between the wrinkles and safe areas, wrinkles tendency areas which is %2.9 of the plate was observed. These wrinkles areas are also observed in the samples taken from the production and do not pose any problem during the life cycle of the component. Because the areas with wrinkles are formed by the areas where the plates will be brazed to each other, those areas are filled with filler material. In addition, it does not affect the performance of the plate heat exchanger as no heat transfer is expected to occur in those regions.

## 6.5. Process Optimization Study

The production quantities of plate heat exchangers, which are utilized in the manufacturing of combi boilers, are generally substantial. In order to enhance cost efficiency in plate heat exchanger production, it is possible to conduct optimization and development studies on the process. Within the framework of this research, an investigation was conducted on the boundary conditions to optimize the process using a developed model. Typically, production facilities aim to reduce production times by increasing the punch speed in the press machine. However, the increase in punch speed is considerably restricted by the strain rate sensitivity of the sheet material employed. The strain rate sensitivity determines the new values for both the failure strain and stress levels obtained in the structure. In this particular study, a plate heat exchanger composed of 316L stainless steel was examined. 316L stainless steel is recognized for its high precision

in terms of strain rate, hence this effect must be taken into account in both the manufacturing process and its numerical simulation.

Sheet metal forming structural analysis simulation can be used for process optimization as well as for comparison of design parameters, material changes, plates of different thicknesses. Therefore, it is also possible to optimize the process to increase production efficiency during the sheet metal forming process. After the model was established, numerical models were run by increasing the punch speed to optimize the processing speed. Considering the Max Effective stress levels, an increase of up to 4 times, followed by a decrease and stabilization were observed.[33] No significant changes were observed in the Max plastic strain levels. Overall, a stable trend following curve was obtained.

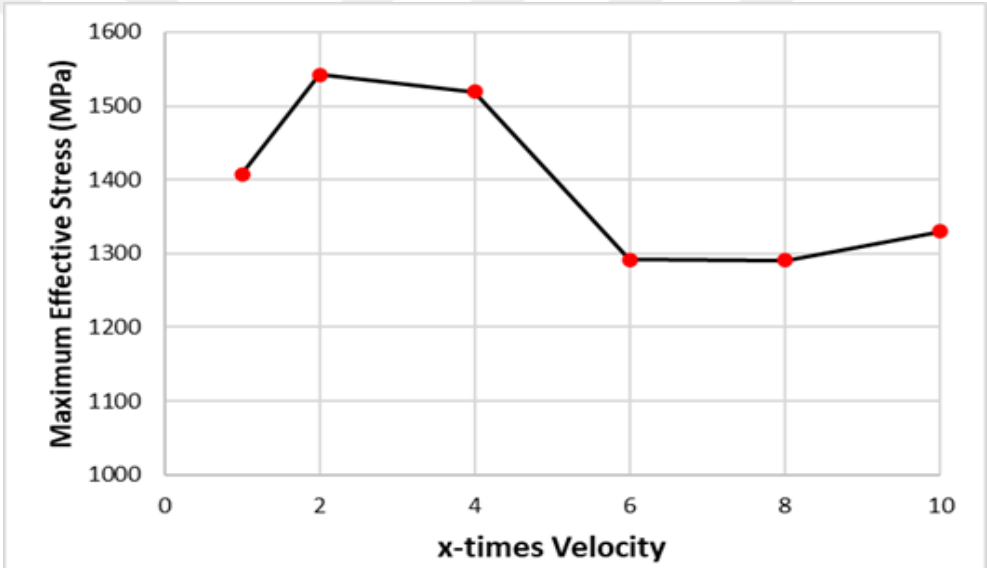


Figure 69. Max effective stress graph of PHE according to x-times punch velocity (Source: Şimşek, İ. et. al, 2022)

Critical parameters for product reliability are the thickness reduction values. Because water passes through high pressures through the final product, a test procedure called water hammer is applied in the final test. The thickness reduction in three different regions was examined. A downtrend was encountered when the velocity increased in the valley region. The same curve was observed for the Hill region and the hole area. The thickness reduction levels decrease as the speed increases.

Based on the optimization study, there are no observed issues with doubling the velocity. However, before implementing a fourfold velocity increase, it is advisable to

assess its impact on the production department. It is recommended to address the optimization of gas spring forces in future research, as the strength of the material improves with higher speeds. The constant gas spring force has an impact on the formability performance. When optimizing the forming process, it is crucial to evaluate the process parameters as a collective rather than individually.

Table 17. Tabular results of thickness reduction in three different regions (Valley, Hill, Hole) according to x-times punch velocity (Source: Şimşek, İ. et. al, 2022)

| Valley | | Hill | Hole |
|---|---|---|---|
| x-times Velocity | Thickness Reduction (%) | Thickness Reduction (%) | Thickness Reduction (%) |
| 1 | 10,87 | 14,05 | 17,19 |
| 2 | 10,63 | 14,00 | 16,90 |
| 4 | 9,62 | 13,80 | 15,89 |
| 6 | 8,44 | 13,50 | 14,77 |
| 8 | 7,94 | 13,10 | 13,83 |
| 10 | 7,63 | 12,60 | 13,08 |

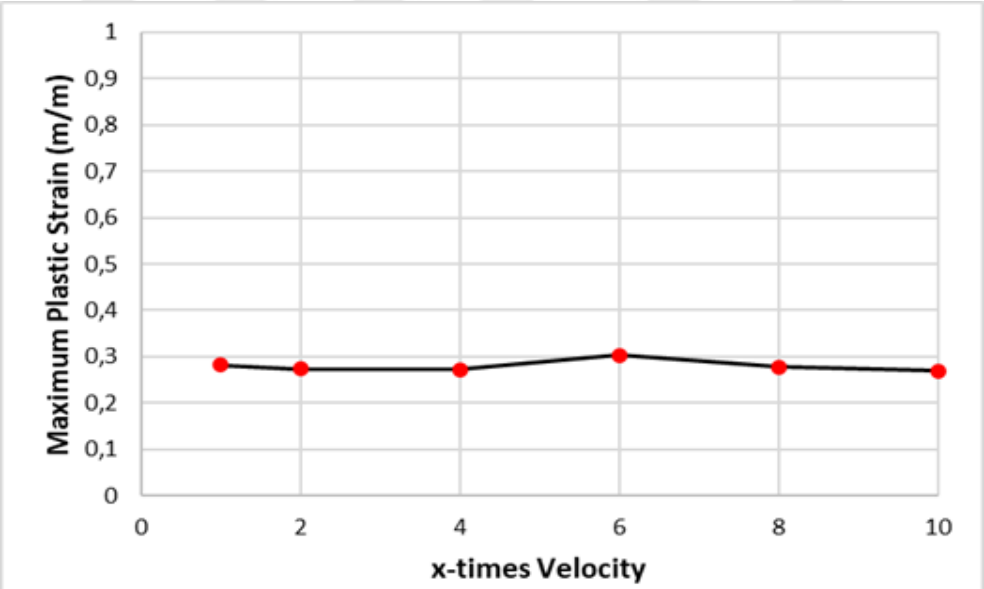


Figure 70. Max plastic strain graph of PHE according to x-times punch velocity (Source: Şimşek, İ. et. al, 2022)

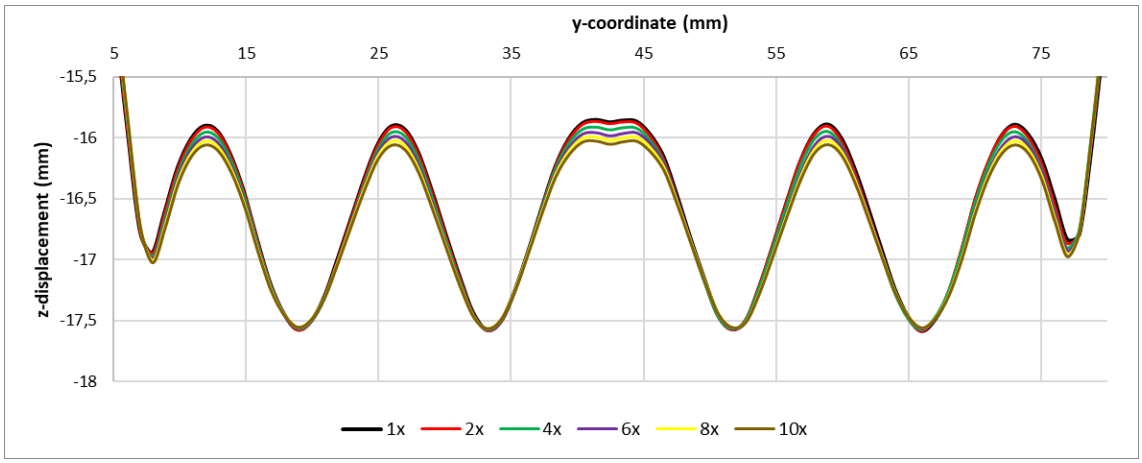


Figure 71. Cross section along the y axis comparison between x-times punch velocities for 316L [33] (Source: Şimşek, İ. et. al, 2022)

# CHAPTER 7

# CONCLUSION

As a conclusion, as mentioned in previous chapters, a sheet metal forming process simulation methodology was developed for plate type heat exchangers. With this developed methodology, a lot of information and know-how gains about the process were obtained. The methodology that emerged because of the experimental and numerical research, in the following periods, the plate heat exchanger component; It will provide the opportunity to observe the effects of the changes by saving time and cost on issues such as design change, material change, process parameter change. The main findings found throughout this study process are as follows.

While developing the sheet metal forming process structural analysis simulation, the most important parameter to be decided at the beginning is the material model. In this methodology, the beginning was made with the selection of the most suitable material model, as made by Maker, B.N., et al, Lazarescu, L., et al, Banabic, D., et al, Deng, Z., et al, and Sener, B., et al, in their studies. During the selection of this material model, uniaxial tensile tests and biaxial hydraulic bulge test data were used in different tensile directions on the material. Subsequently, uniaxial tensile tests and biaxial hydraulic bulge tests were modeled in numerical environment. *MAT133_BARLAT_YLD2000 and *MAT093_SIMPLIFIED_JOHNSON_COOK material models identified as candidates were created using test data. The major factor and common feature of the *MAT133_BARLAT_YLD2000 and *MAT093_SIMPLIFIED_JOHNSON_COOK material models as candidates are that it defines the strain rate sensitivity parameter in both material models. The aim here is to learn the effect of the material's anisotropic behavior in the numerical environment. Our outputs were progressed with the material card, which gives the most accurate result according to the behavior of our material, as performed by by Maker, B.N., et al, Lazarescu, L., et al, Banabic, D., et al, Deng, Z., et al, and Sener, B., et al, in the literature. As a result, the material model *MAT133_BARLAT_YLD2000 was selected. Because the main difference between *MAT133_BARLAT_YLD2000 and *MAT093_SIMPLIFIED_JOHNSON_COOK is that the *MAT093_SIMPLIFIED_JOHNSON_COOK material model starts to deviate with experimental data at 0.35 strain and above.

During the metal forming process and after the springback process, the stress values on the plate were investigated. Among these stress values, the maximum effective stress value observed during the process is 1408 MPA for AISI 316L stainless steel and 1204 MPA for AISI 304 stainless steel. Accordingly, the plastic strain values formed on the plate made of two different materials are maximum 0.28 and 0.26 for AISI 316L and AISI 304, respectively. The result is that AISI 316L stainless steel is more deformed and has maximum stress. On the other hand, residual stress values were determined in the plates with spring-back analysis, and it is maximum 1124 MPA for AISI 316L stainless steel and 1138 MPA for AISI 304 stainless steel. According to the results, although AISI 316L stainless steel is subjected to more stress at forming than AISI 304 stainless steel, the stress levels after springback are quite close to each other. This is due to the fact that AISI 316L stainless steel is a more ductile material than AISI 304 stainless steel.

Ensuring product reliability of the component is one of the output of this study. For this reason, as the output of the study, the thickness reduction values, and thickness distribution formed after the forming process on the plate were examined. When the thickness distribution was examined, the minimum thickness value observed for the AISI 316L stainless steel material was found to be 0.23 mm. In the same way, it was determined as 0.25 mm in the examinations made of AISI 304 stainless steel material. In accordance with the internal standards of the company, a thickness reduction limit has been determined in order to eliminate the possibility of internal and external leakage. Since this limit is the know-how within the company, it cannot be shared here. However, the minimum thickness values obtained from the simulation results remain within these limits. On the other hand, thickness reduction value, which is another parameter examined, was also examined separately for 3 different regions, and compared between materials. As mentioned in the previous chapters, these regions are the critically selected Valley, Hill, and Hole regions. Thickness reduction values taken from the same points for both materials are the same. When the Valley region is examined, 10.87% and 9.45% thickness reduction was observed for 316L and 304 stainless steel material respectively. When the Hill region is examined, 14.05% and 12.2% thickness reduction is observed for 316L and 304 stainless steel material respectively. When the Hole area is examined, 17.19% and 13.5% thickness reduction is observed for 316L and 304 stainless steel material respectively. As a result of the two parameters examined, under the same boundary conditions, 316L stainless steel undergoes more deformation and shows more examination, while 304 stainless steel undergoes less deformation and thinning rate is

observed less. The conclusion to be drawn here may be that 304 stainless steel behaves more durable, but at this point formability comes into play. Because at the end of the day, both materials remained within the specified safe limits. Forming performances were examined and compared on cross sections. When the forming performances are examined, while 316L stainless steel can take the desired final geometry form, 304 stainless steel has undergone form deviations in critical areas of the final geometry. Another valuable comment to be taken from here is that the process parameters for 304 stainless steel should be optimized again and the gas spring forces and punch speeds used should be revised so that it takes the form. Under the same boundary conditions, 316L stainless steel has a better form-taking performance than 304 stainless steel, because the material has a more ductile feature.

No crack or crack risk was observed after the forming process, when the numerical analysis results for 316L stainless steel were compared with the forming limit diagram. The results were calculated as a percentage over the number of formed elements of the plate and calculated as 73.7% safe area, 11.9% inadequate stretch area, 11.5% wrinkles area and 2.9% wrinkles pattern area. With 73.7%, it was observed in the area where the safe area plate is in contact with the other plates, and it was observed to be successful because heat transfer took place in this area. The remaining 11.9% inadequate stretch area, 11.5% wrinkles area and 2.9% wrinkles tendency areas were observed in the edges and holes of the plate. These regions will be subject to brazing in assembly state. The occurrence of wrinkles or wrinkles pattern in these areas does not pose any risk in terms of reliability of the product. In addition, since the pattern area is safe, it does not affect the heat transfer and has a successful design.

The determination of the numerical parameters to be used while developing the sheet metal forming process simulation methodology was determined by examining the literature and Ls-Dyna manuals. In addition, the implementation of the effects of boundary conditions to the model was studied. Maker, B.N. and Zhu, X., with the publication Input Parameters for Metal Forming Simulations using LS-DYNA, similar parameters were also used in this study. In the study, it was observed that the parameters that should be considered and recommended are important. In addition to other sheet metal forming simulations in the literature, gas springs with a movable punch and die were defined in the model created in this study. However, strain rate sensitive, which was not included in the modeling in the Deformation Optimization of Plate Heat Exchangers study by Noren, M. in the literature, was included in the model in this study. Numerical

model with included strain rate sensitivity effect; In addition to being used for design optimization, material change or selection, it has also been made usable for process optimization studies. With the process optimization study carried out in this study, the punch speed was increased to 2x, 4x, 6x, 8x, 10x. The results were analyzed on effective stress, effective plastic strain, and thickness reduction. No risk was observed for a 2x velocity increase. For 4x velocity increase can be selected by evaluating it on the production department. It was concluded that for comprehensive optimization studies, it would be appropriate to conduct a study that includes all the parameters and boundary conditions affecting the process.

Future studies, the preparation of the forming limit diagram (FLD) for 304 stainless steel and the evaluation of the results are planned among future studies. In addition, considering the current material supply problems, test and simulation studies can be carried out for alternative plate heat exchanger materials.

In addition, an optimization study can be performed in which major parameters affecting the forming process, such as gas spring force, punch velocity, etc. With this work to be carried out, the number of plates to be produced in unit time can be increased and the production cost can be reduced.

# REFERENCES


1. Atılım University Metal Excellence Center. Bosch Metal Test Report. 2015.

2. fka GmbH. Fka Metal Test Report. 2022.

3. Hallquist, J. O. LS-DYNA® keyword user's manual Volume II material models. Livermore, California, USA, 2013.

4. Worcester Bosch. Greenstar 2000 [Photograph]. Retrieved from https://www.worcester-bosch.co.uk/professional/products/boilers/greenstar-2000 (Accessed: 2023).

5. Worcester Bosch. Boilers Explained [Photograph]. Retrieved from https://www.worcester-bosch.co.uk/products/boilers/explained (Accessed: 2023).

6. Gürler, Y. Design and mechanical behaviour of brazed plate heat exchangers. Master's thesis, Izmir Institute of Technology, Izmir, Turkey, 2018.

7. Abou Elmaaty, T. M., Kabeel, A. E., & Mahgoub, M. Corrugated plate heat exchanger review. Renewable and Sustainable Energy Reviews, 70, 852-860, 2017.

8. Hayta, Y. Investigation of the fatigue behaviour of metallic components used in plate heat exchangers under variable dynamic loads. Master's thesis, İzmir Institute of Technology, İzmir, Turkey, 2020.

9. Gürler, Y., Şimşek, İ., Savaştaer, M., Karakuş, A., & Taşdemirci, A. Comparison of Johnson-Cook and Barlat Material Model for 316L Stainless Steel. 2021.

10. Maker, B. N., & Zhu, X. Input Parameters for Metal Forming Simulations using LS-DYNA. Livermore Software Technology Corporation, April 2000.

11. Maker, B. N., & Zhu, X. Input Parameters for Springback Simulations using LS-DYNA. Livermore Software Technology Corporation, June 2001.

12. Lazarescu, L., Ciobanu, I., Nicodim, I. P., Comsa, D. S., & Banabic, D. Effect of the mechanical parameters used as input data in the yield criteria on the accuracy of the finite element simulation of sheet metal forming processes. In Key Engineering Materials (Vol. 554, pp. 204-209). Trans Tech Publications Ltd, 2013.

13. Banabic, D., & Sester, M. Influence of material models on the accuracy of the sheet forming simulation. Materials and Manufacturing Processes, 27(3), 273-277, 2012.

14. Deng, Z., & Hennig, R. Influence of material modeling on simulation accuracy of aluminum stampings. In Journal of Physics: Conference Series (Vol. 896, No. 1, p. 012025). IOP Publishing, September 2017.

15. Sener, B., Kilicarslan, E. S., & Firat, M. Modelling Anisotropic Behavior of AISI 304 Stainless Steel Sheet Using a Fourth-Order Polynomial Yield Function. Procedia Manufacturing, 47, 1456-1461, 2020.

16. Norén, M. Deformation Optimization of Plate Heat Exchangers. 2016.

17. Tasdemirci, A., Sahin, S., Kara, A., & Turan, K. Crushing and energy absorption characteristics of combined geometry shells at quasi-static and dynamic strain rates: Experimental and numerical study. Thin-Walled Structures, 86, 83-93, 2015.

18. Sigvant, M., Pilthammar, J., Hol, J., Wiebenga, J. H., Chezan, T., Carleer, B., & van den Boogaard, T. Friction in sheet metal forming: Influence of surface roughness and strain rate on sheet metal forming simulation results. Procedia Manufacturing, 29, 512-519, 2019.

19. Lee, S. W., & Yang, D. Y. An assessment of numerical parameters influencing springback in explicit finite element analysis of sheet metal forming process. Journal of Materials Processing Technology, 80, 60-67, 1998.

20. Panthi, S. K., Ramakrishnan, N., Ahmed, M., Singh, S. S., & Goel, M. D. Finite element analysis of sheet metal bending process to predict the springback. Materials & Design, 31(2), 657-662, 2010.

21. Pham, Q. T., Song, J. H., Park, J. C., & Kim, Y. S. Investigation of springback prediction for an aluminum 7000 sheet subjected to press forming. In Applied Mechanics and Materials (Vol. 889, pp. 203-210). Trans Tech Publications Ltd, 2019.

22. Dharavath, B., Morchhale, A., Singh, S. K., Kotkunde, N., & Naik, M. T. Experimental Determination and Theoretical Prediction of Limiting Strains for ASS 316L at Hot Forming Conditions. Journal of Materials Engineering and Performance, 29(7), 4766-4778, 2020.

23. Park, N., Huh, H., Lim, S. J., Lou, Y., Kang, Y. S., & Seo, M. H. Fracture-based forming limit criteria for anisotropic materials in sheet metal forming. International journal of plasticity, 96, 1-35, 2017.

24. Pilthammar, J., Schill, M., Sigvant, M., Sjöblom, V., & Lind, M. Simulation of Sheet Metal Forming using Elastic Stamping Dies. 2019.

25. Turan, A. K. The penetration behavior of repeated hemisphere core sandwich structures: An experimental and numerical study (Doctoral dissertation, Izmir Institute of Technology (Turkey)), 2018.

26. Irizalp, S. G., & Saklakoglu, N. High strength and high ductility behavior of 6061-T6 alloy after laser shock processing. Optics and Lasers in Engineering, 77, 183-190, 2016.

27. FormingWorld. Sheet Metal Plasticity Visualized (Part 1 of 2) [Photograph]. Retrieved from https://formingworld.com/sheet-metal-plasticity-visualized-part-1-of-2/ (Accessed: 2023).

28. Hu, J., Marciniak, Z., & Duncan, J. (Eds.). Mechanics of sheet metal forming. Elsevier, 2002.

29. Quiri. [Photograph]. Retrieved from https://www.quiri.com/en/ (Accessed: 2023).

30. Altan, T., & Tekkaya, A. E. (Eds.). Sheet metal forming: fundamentals. Asm International, 2012.

31. Groche, P., Filzek, J., & Nitzsche, G. Local contact conditions in sheet metal forming and their simulation in laboratory test methods. Wissenschaftliche Gesellschaft Für Produktiontechnik (in Braunschweig), 11(1), 55-60, 2004.

32. Lee, W. S., Chen, T. H., Lin, C. F., & Luo, W. Z. Dynamic mechanical response of biomedical 316L stainless steel as function of strain rate and temperature. Bioinorganic chemistry and applications, 2011.

33. Şimşek, İ., Gürler, Y., & Taşdemirci, A. The Investigation of the Effect of Punch Velocity Increment on the Thickness Reduction of PHE Plates. In 16th LS-DYNA Forum 2022.

34. Poceski, A. Fundamentals of the Finite Element Method. In Mixed Finite Element Method (pp. 15-73). Berlin, Heidelberg: Springer Berlin Heidelberg, 1992.

35. Simultura Material Technologies. Surface Residual Stress Measurement Report. 2023.

36. LSTC. LS-DYNA Theory Manual. 2022.

37. Hallquist, J. O. LS-DYNA KEYWORD USER'S MANUAL Volume I. Livermore Software Technology Corporation, 2009.

38. Gutscher, G., Wu, H.-C., Ngaile, G., & Altan, T. Determination of flow stress for sheet metal forming using the viscous pressure bulge (VPB) test. Journal of Materials Processing Technology, 146(1), 1-7, 2004.

39. Koh, C. Design of a Hydraulic Bulge Test Apparatus. Department of Mechanical Engineering at Massachusetts Institute of Technology, 2012.